Article

Main Controlling Factors and Models of Organic Matter Accumulation in Lower Carboniferous Dawuba Formation Shale in Southern Guizhou, China

Jialiang Niu, Jinchuan Zhang,* Xuan Tang,* Kun Yuan, Tuo Lin, Yang Liu, Yanjie Niu, Pei Li, Xingqi Li, and Yutao Liang

Read Online

ACCESS | Metrics & More | Article Recommendations | SI Supporting Information

ABSTRACT: A set of high-quality marine facies organic-rich shales developed in the Lower Carboniferous Dawuba Formation, which is considered to be the main target of shale gas exploration and development in Guizhou Province. In this paper, 53 samples from Well ZY1 are selected, and the core observation data, field-emission scanning electron microscopy (FE-SEM) images, and geochemical data of these samples are analyzed. On the basis of these data, the main influencing factors of organic matter enrichment in the Dawuba Formation shale were identified and an organic matter accumulation model was established. The results show that total organic carbon (TOC) values of the Dawuba Formation in the ZY1 well vary between 1.97 and 4.11%, with high values appearing at the depths of 2796−2814 m (3.00−4.11) and 2877−2894 m (1.97−3.49). The redox-sensitive element enrichments are generally low, indicating that these samples were deposited under oxic−suboxic conditions. The micronutrients (Zn, Cu, and Ni), biological Ba (Ba_{XS}), and P/Al also show low values, indicating low primary productivity. The chemical index of alteration (CIA) and terrigenous clastic input index (Ti/Al) showed two obvious high-value zones, indicating that shale in the study area was affected by terrigenous inputs. Similarly, the calculation results show that Fe/Mn and Rb/K values have two abnormal data segments at the same depth. The anomaly of these data at the same depth section further suggests that the shale was affected by terrigenous input during deposition. Moreover, the terrigenous input reaches the maximum in the above TOC high-value region, and it is inferred by combining with the core observation results that the gravity flow occurs in this depth. The carbon isotope of kerogen ($\delta^{13}C_{org}$) ranges from −26.84 to −24.36%, indicating that the source of organic matter is likely to be terrestrial plants. This is further supported by the widespread presence of filamentous organic matter using FE-SEM, despite the low productivity and poor preservation conditions during deposition of the Dawuba Formation; the enhanced terrigenous input may have provided additional sources of organic matter for the Dawuba shale.
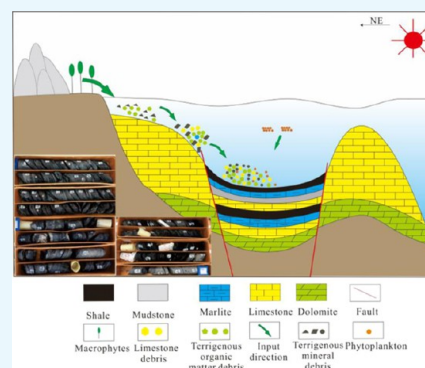
1. INTRODUCTION

As an important source rock and the main producing layer of shale gas, black organic-rich shale plays a dominant role in oil and gas exploration and development. With the deepening of research, the main controlling factors and modes of organic matter accumulation in shale have also attracted much attention.[1−10] Based on this, the researchers established a productivity model for upwelling zones at continental margins, such as the modern Arabian Sea. These models take high marine primary productivity and sink fluxes of organic carbon as the key points to illustrate the accumulation modes of organic matter in the strata of high-productivity areas.[11,12] As the study progressed, the researchers found that marine primary productivity alone could not fully explain the characteristics of organic matter accumulation in some areas.[13] As a result, geologists developed conservation models suitable for low productivity and stagnant waters, such as the modern Black Sea. In this model, more attention is paid to the effects of reduction conditions and the reduction of oxidation decomposition of sinking organic particles on the enrichment of organic matter.[14,15] However, with the further development of oil and gas exploration, these two organic matter accumulation models are not fully applicable in some areas, which makes researchers begin to pay attention to the influence of terrigenous input on organic matter accumulation.[16] However, there is no consensus as to whether terrigenous input is beneficial to the accumulation of organic matter in the strata, but it has been widely recognized by researchers that it will affect the accumulation of organic matter.[3,17,18]
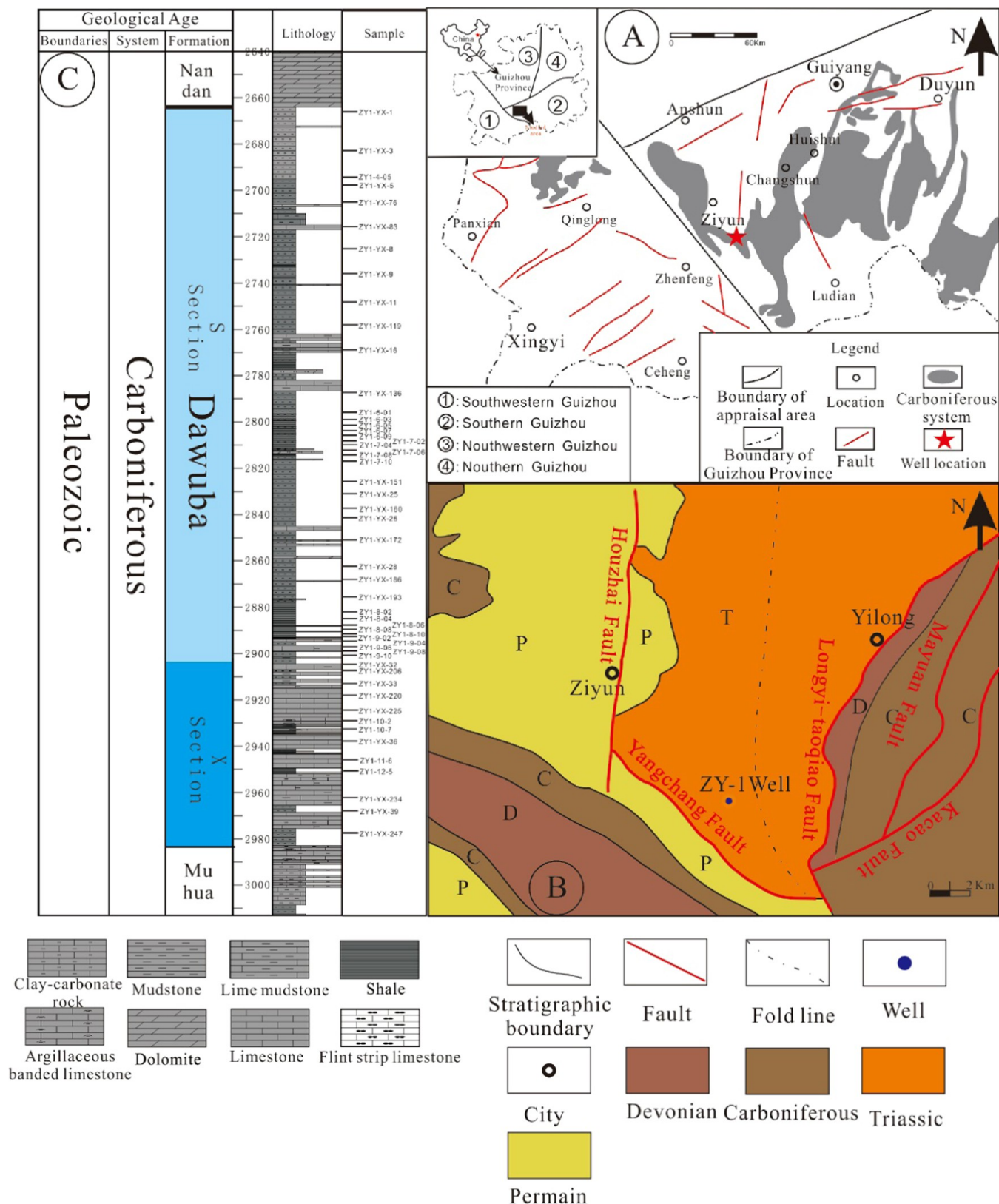
Figure 1. Stratigraphic histogram and the location and geological map of the Ziyun region. (A) Location of the Southern Down warping in Guizhou and Ziyun regions, (B) geological map of the Ziyun region and the shale Well locations, and (C) Simplified stratigraphic unit of the ZY1 well profile.

The Qiannan Depression is located in the Upper Yangtze Plate, where a set of organic-rich shales of the Lower Carboniferous Dawuba Formation is deposited in the platform basin facies,[19,20] and it is the main hydrocarbon source rock in Southwest China.[21,22] Previous studies show that the shale of the Dawuba Formation is characterized by the low content of

brittle minerals, high content of clay minerals, high maturity (between 2.0 and 3.0), and relatively high abundance of organic matter (generally greater than 2.0), thus providing favorable conditions for shale oil and gas enrichment.[23−25] Wells CY-1, DY-1, and ZY1, all of which have been completed at present, have found good shale gas display in the formation of the Dawuba Formation.[24,26,27] This indicates that some achievements have been made in the Lower Carboniferous Dawuba Formation in the Qiannan Depression, but it cannot be regarded as a major breakthrough in shale gas exploration in the Upper Yangtze area.[28−30] At present, the research on the shale of the Lower Carboniferous Dawuba Formation mainly focuses on the reservoir characteristics, hydrocarbon source rock evaluation, shale gas resource potential prediction, etc.[31−34] There are few studies on the main controlling factors and models of organic matter accumulation in this geological background. At present, Ding (2018) and a few others have discussed the main controlling factors and modes of organic matter accumulation in the Lower Carboniferous Datang Formation shale in the southern Guizhou depression from the aspects of paleoproductivity and reoxidation−reduction conditions and believe that paleoproductivity is the main controlling factor of organic matter enrichment. However, this model still cannot fully explain all of the characteristics of organic matter enrichment in black shale of the Lower Carboniferous Dawuba Formation in southern Guizhou. In addition, organic matter plays an important role in controlling hydrocarbon generation potential, pore structure, and adsorption capacity of organic-rich shale.[35−37] Therefore, to better understand the characteristics of shale gas accumulation in the Dawuba Formation, it is necessary to clarify the main controlling factors and modes of organic matter accumulation in this geological background.

In this paper, the total organic carbon (TOC), major element (ME), and trace element (TE) were measured for the samples from the Dawuba Formation of Well ZY1. In addition, combined with core observation data, field-emission scanning electron microscopy (FE-SEM) images, and logging data, the characteristics of paleoproductivity, paleoredox environment, and terrigenous debris input during the deposition of the Dawuba Formation were analyzed, and the organic matter enrichment model suitable for the study area was established.

2. GEOLOGICAL BACKGROUND

The study area is located in the south of Guizhou Province, Southwest China (Figure 1A). Tectonically, it belongs to the Qiannan Depression on the southwest margin of the Upper Yangtze Plate and has undergone multiple complex tectonic movements, forming a series of NW-trending axial folds and NW- or NE-trending faults.[21,38] The main outcrop strata in this area are Devonian, Carboniferous, and Permian. A large set of black shale developed in the Upper Yangtze region during the Early Carboniferous due to a large-scale sea-level rise in the Upper Yangtze region and its surrounding areas,[20,21] which resulted in the formation of an intraplatform basin with a relatively shallow water depth in the front depression of southern Guizhou.[20] In the study area, the Lower Carboniferous has a wide distribution area and unconformity contact with the underlying Devonian system. The whole Carboniferous strata can be divided into three stratigraphic units. The upper part of the Nandan Formation mainly develops a set of limestone with a thickness of 800−900 m; the lower part of the Muhua Formation also develops a set of limestone with a

thickness of 0−300 m; and the middle part of the Dawuba Formation, which is the horizon of this study, mainly develops shale, siliceous rock, calcareous shale, and argillaceous shale with a thickness between 90 and 300 m, and it belongs to shallow shelf sedimentary facies.

The ZY1 well is located in the western margin of the southern region of Guizhou Province. The main outcropping strata in the drilling area are the Devonian, Carboniferous, Permian, and Triassic strata (Figure 1B). The drilling depth of the entire ZY1 was 3050 m, and the completed drilling horizon was Wuzhishan Formation. The strata drilled from top to bottom were Luolou Formation of the Lower Triassic, Linghao Formation of the Upper Permian, Sidazhai Formation of the Lower Permian, Nandan Formation of the Upper Carboniferous, Haohua Formation of the Lower Carboniferous, and Wuzhishan Formation of the Upper Devonian. Among them, the Muhua and Nandan Formations mainly developed large sets of limestone, while the Dawuba Formation mainly developed shale, siliceous rock, calcareous shale, and argillaceous shale (Figure 1C). The depth of the drilled well in the Dawuba formation is 2770−2983 m, and the layer thickness is 231 m. According to the lithology encountered during drilling, the whole Dawuba Formation in Well ZY1 can be divided into upper mudstone (section S), shale, and thin-bedded limestone section and lower clastic limestone and thin-bedded mudstone section (section X) (Figure 1A).

3. SAMPLES AND METHODS

3.1. Samples. All 53 samples were collected from Well ZY1 at a depth of 2688−2976 m. The samples included mudstone, shale, marl, and dolomite. The sample number, depth, and lithology are listed in the attached table. Each sample collected was rinsed with deionized water to remove mud contamination during drilling. The selection of samples is mainly mudstone and shale, and under the premise of maintaining a certain sampling interval, all of the depths of the whole Dawuba Formation should be covered as far as possible. Samples were analyzed in the terms of TOC, major and trace elements, and FE-SEM. At the same time, 26 samples were selected from top to bottom for the carbon 13 isotope test of kerogen ($\delta^{13}C_{org}$), and the samples were selected as far as possible to cover all depths of the Dawuba Formation.

3.2. Experimental Methods. After removing the potential weathering layer, sedimentary veins, and visible pyrite nodules on the surface of 53 samples, some samples were selected for scanning electron microscopy observation, and the rest were crushed to about 200 mesh for geochemical analysis. The geochemical experiments were all completed in China University of Geosciences (Beijing), and scanning electron microscopy observation was performed at China University of Petroleum (Beijing).

All 53 rock samples were crushed to a size of less than 200 mesh. About 2 g of powder was placed in a porous crucible and treated with hydrochloric acid (50%) to remove inorganic carbon. The remaining residue was rinsed with deionized water to neutral pH, centrifuged, and dried. Finally, a 902T C-S analyzer (China University of Geosciences, Beijing, China) was used to analyze the TOC data of the sample.

For analysis of major elements (MEs), the sample powder was heated to 105 °C and then baked at 920 °C to completely remove the organic components from the sample. The heated sample powder was then mixed with $Li_2B_4O_7$ and $BliO_2$ and fused on a glass table at 1150 °C. Then, an X-ray fluorescence
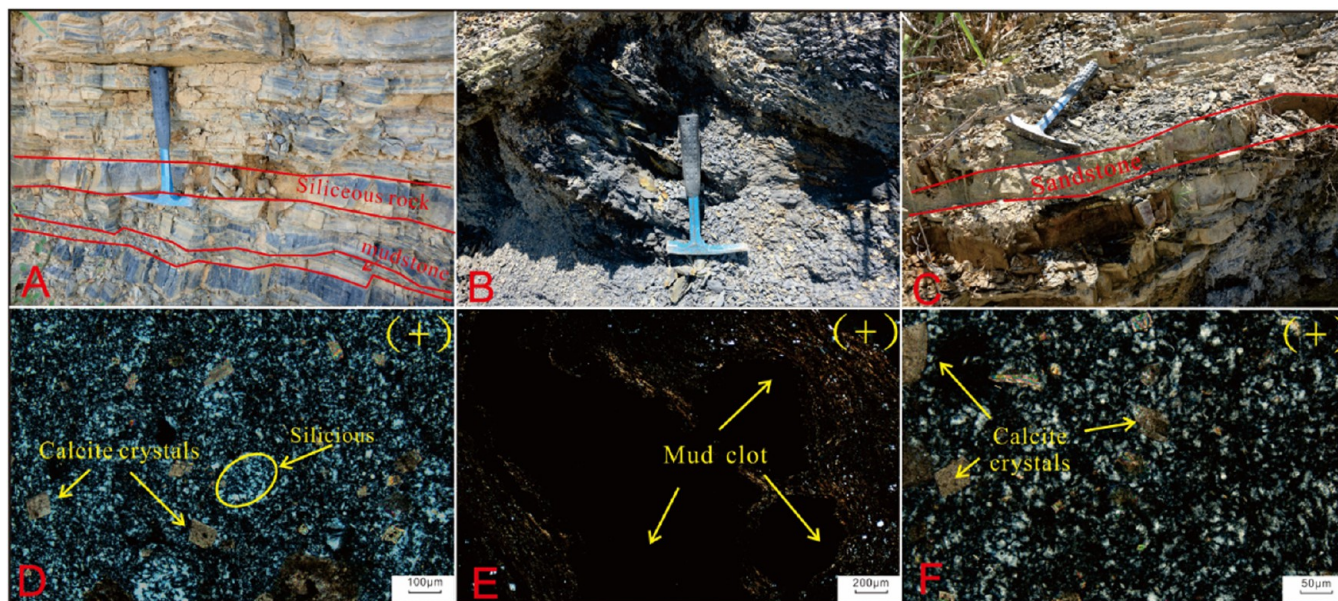
Figure 2. Photographs displaying major lithofacies of the Dawuba Formation. Panels A−C are photographs from outcrops of the Dawuba Formation, whereas D−F are thin-section micrographs. (A) Siliceous rocks interbedded with mud shale, in which the mud shale is thin and has undergone strong weathering. (B) Black organic-rich shale with a slightly weathered surface. (C) Pale yellow sandstone with normal grain sequence. (D) Thin section of siliceous rock with yellowish calcite crystals can be observed. (E) Thin section of mud shale in which visible near-circular mud clots can be seen. (F) Thin section of sandstone in which calcite crystals can be observed. (+) represents cross-polarized light; (−) represents plane-polarized light.

spectrometer (Analymate V8C instrument) was used to measure the content of major elements in the samples on molten glass. The precision of the whole experiment was guaranteed at ±5%. For detailed main element analysis experiment steps, refer to Cao et al.[39]

For analysis of trace elements (TEs), a PE NexION 350X Inductively Coupled Plasma-Mass Spectrometry (ICP-MS) instrument was used. The sample powder was dipped in mixed acid ($HF/HNO_3/HClO_4$ = 1:1:3) in a pressurized sample tank at 200 °C for 12−24 h. Then, the liquid was measured by inductively coupled plasma-mass spectrometry (ICP-MS) to obtain the trace element content of the sample. Detailed experimental steps were carried out by Liu et al.[40]

For scanning electron microscopy, first, the sample was cut into 2 cm² tetrodes slices. Then, the sample was ground with fine sandpaper and polished with an argon ion beam to produce a flat surface. Finally, the sample was observed with a Zeiss FE-SEM electron microscope and photographs were obtained.

To observe the thin section of rock, first, the sample was cut into 2 cm² tetrodes slices. Then, the sample was ground with fine sandpaper to produce a flat surface. Meanwhile, the differentiated layer on the sample surface was removed. Finally, the sample was observed with a Zeiss polarizing microscope and photographs were obtained.

3.3. Analytical Methods. To more accurately analyze the paleoredox conditions, paleoproductivity, and terrestrial input in the study area, the geochemical data were calculated and processed, including the element enrichment coefficient (X_{EF}), chemical weathering index (CIA), biological barium (Ba_{XS}) Ti/Al, Fe/Mn, Rb/K, and P/Al, respectively.

The calculation formula for the element enrichment coefficient is as follows

$$X_{EF} = [(X/Al)_{sample}/(X/Al)_{AUCC}]$$

where $(X/Al)_{sample}$ represents the ratio of X element to Al element in the sample and $(X/Al)_{AUCC}$ represents the ratio of the average content of X element to the average content of Al element in the upper crust.[41]

The chemical weathering index (CIA) calculation formula[42,43] is

$$CIA = [Al_2O_3/(Al_2O_3 + CaO^* + Na_2O + K_2O)] \times 100$$

It needs to be emphasized that the unit of major element (ME) oxides in the above-mentioned expression is mole, and CaO^* merely represents the CaO originated from silicate minerals. However, to avoid the CaO content in the rock is composed of carbonate and phosphorite, it is necessary to correct the CaO content. The correction formula is as follows

$$CaO^* = CaO - P_2O_5 \times 10/3$$

When the "remaining number of moles" was more than that of Na_2O, the mole of CaO^* was supposed to be equivalent to that of Na_2O. Otherwise, the mole of CaO was regarded as that of CaO^*.[44−46]

The calculation formula of biological Ba (Ba_{XS})[47] is as follows

$$Ba_{XS} = Ba_{total} - (Al \times Ba_{AUCC}/Al_{AUCC})$$

In the above formula, Ba_{total} represents the total barium content in the sample, Al represents the total Al content in the sample, and Ba_{AUCC} and Al_{AUCC} represent the average Ba and Al contents in the upper crust, respectively.[41]

4. RESULTS

4.1. Field Section and Microscopic Section Observation. Based on the data collected from previous Wells and outcrops, three outcrops were observed and described in this study.
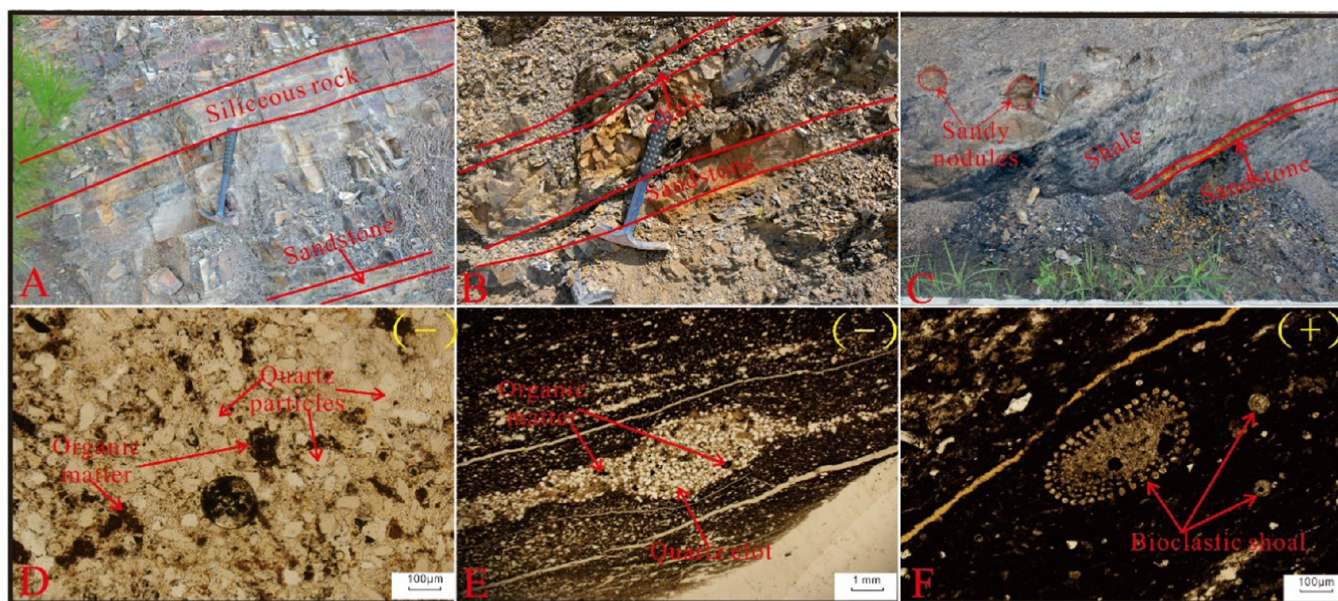
Figure 3. Photographs displaying major lithofacies of the Dawuba Formation. Panels A−C are photographs from outcrops of the Dawuba Formation, whereas D−F show the thin-section micrographs. (A) Siliceous rocks interbedded with sandstone. (B) Sandstone is interbedded with mudstone, among which mudstone is highly weathered, and sandstone is of normal grain sequence. (C) Black organic-rich shale interbedded with thin sandstones and sandy nodules were observed in the section. (D) Thin section of siliceous rock with black organic matter can be observed. (E) Thin section of mud shale in which visible quartz clots can be seen. (F) Thin section of mud shale in which bioclastic shoal can be observed. (+) represents cross-polarized light; (−) represents plane-polarized light.
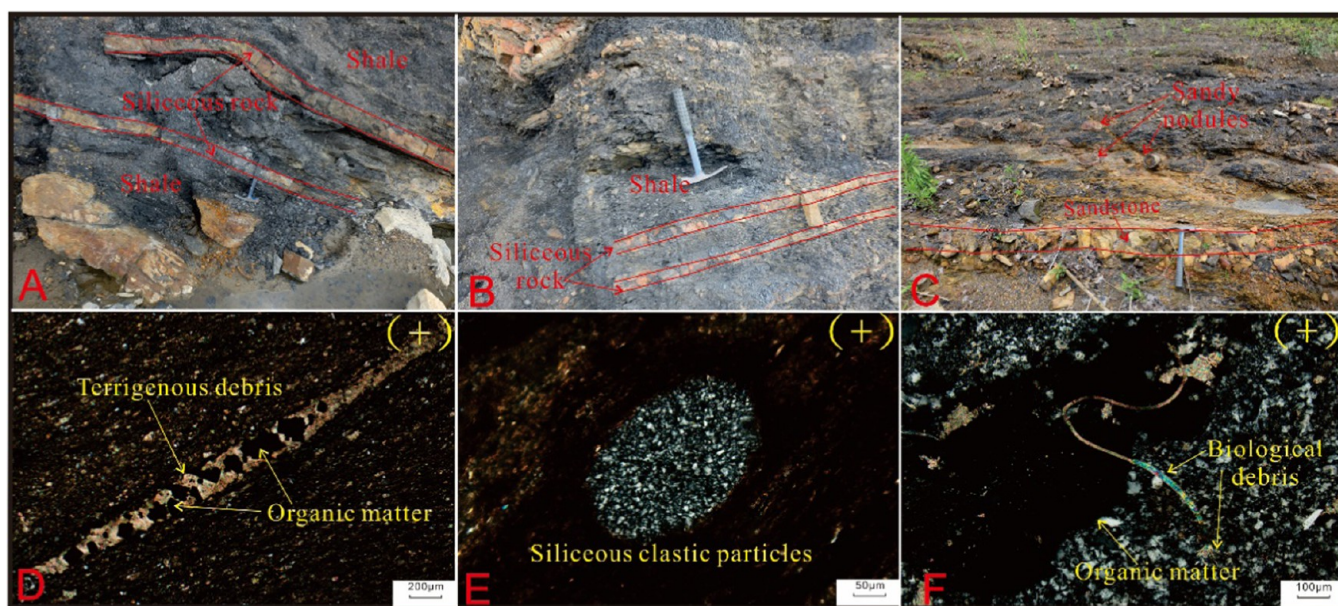

Figure 4. Photographs displaying major lithofacies of the Dawuba Formation. Panels A−C are photographs from outcrops of the Dawuba Formation, whereas D−F show the thin-section micrographs. (A) Siliceous rocks interbedded with mud shale. (B) Siliceous rocks interbedded with mud shale, and wavy bedding can be observed in the section. (C) Black organic-rich shale interbedded with thin sandstones and sandy nodules were observed in the section. (D) Thin section of mudstone in which terrigenous debris containing organic matter can be observed. (E) Thin section of mud shale in which visible siliceous clastic particles can be seen. (F) Thin section of siliceous rock with black organic matter and bioclastic shoal can be observed. (+) represents cross-polarized light; (−) represents plane-polarized light.

4.1.1. Ziyun Sidazhai section. The strata of the Dawuba Formation are completely exposed, with both top and bottom visible and gradually integrated contact with the upper and lower layers. The overlying Nandan Formation is dark gray micritic bioclastic limestone, and the underlying Muhua Formation is gray-white massive limestone with the calcite belt. The Dawuba Formation is mainly composed of black and

gray-black carbonaceous argillaceous and siliceous rocks, intermixed with a small amount of gray and gray-yellow mudstone, silt-fine sandstone, argillaceous siltstone, and silty mudstone. The silt-fine sandstone has a positive grain order, and its abrupt contact with surrounding rock has the characteristics of gravity flow (Figure 2).
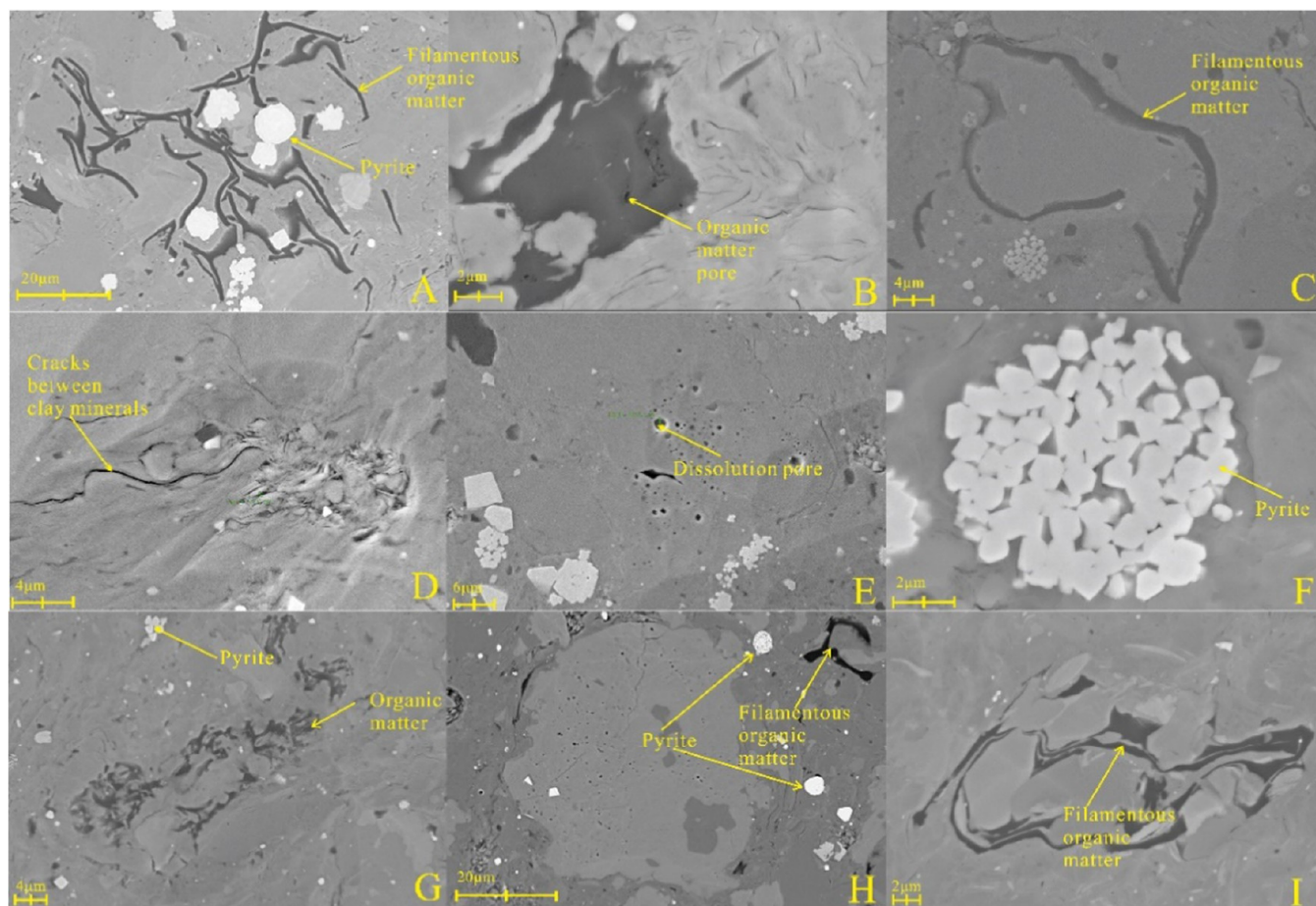
Figure 5. Scanning electron microscopy photo of the Lower Carboniferous DWB Formation. (A) Strawberry pyrite and filamentous organic matter at a depth of 2798.4 m, (B) mass organic matter and pore of organic matter at a depth of 2801.2 m, (C) filamentous organic matter at a depth of 2808.4 m, (D) gap between clay minerals and clay minerals at a depth of 2812.2 m, (E) dissolved pore at a depth of 2826.5 m; (F) strawberry pyrite at a depth of 2832.2 m, (G) strawberry pyrite and filamentous organic matter at a depth of 2880.6 m, (H) strawberry pyrite and filamentous organic matter at a depth of 2890.4 m, and (I) filamentous organic matter at a depth of 2893.7 m.

The Dawuba Formation in the Ziyun Manchang section is completely exposed, with the clastic limestone of Nandan Formation overlying and the gray-black medium-thin marl of Muhua Formation underlying. In the Dawuba Formation, black carbonaceous shales, siliceous rocks, and siltstones are mainly developed, and a small amount of limestone interbeds are also developed. The sandstone layer is in positive grain order, and the sandy combination can be seen in the sudden contact with the surrounding rock. The shale has wavy bedding in which sandy nodules are developed and has the characteristics of gravity flow deposition (Figure 3).

The Getuhe section has a complete outcrop with a visible top and bottom. Nandan Formation is covered by gray massive limestone, and Muhua Formation is covered by gray micritic limestone. In the Dawuba Formation, black carbonaceous shales and siliceous rocks are mainly developed, while small amounts of yellow sandstone interbeds and argillaceous limestones are developed. Mud shale has wavy bedding in which sandy nodules are developed, which is gravity flow deposition (Figure 4).

4.2. FE-SEM Images. The FE-SEM photos show that the organic matter in the samples of the Dawuba Formation is mainly filamentous, as shown in Figure 5A,C,I. However, lumplike organic matter can be seen in a few samples, as shown in Figure 5B. Pyrite is often developed around the filamentous

organic matter, and organic pores are almost not developed in filamentous organic matter. According to FE-SEM images, both strawberry pyrite and euhedral pyrite are developed in the shale samples, and the particle size of strawberry pyrite is between 2 and 10 μm, which reflects the oxygen-poor environment in the upper part of the water.[48] Bulk organic matter is observed in Figure 5B, along with organic pores. However, in all FE-SEM images, clumps of organic matter are rarely developed, which is the reason that organic pores are poorly developed in shale. Finally, a large number of mineral dissolution pores and cracks between clay minerals were observed in the scanning electron microscopy photos, as shown in Figure 5D,E.[49,50]

4.3. Organic Geochemistry. In this experiment, a total of 53 samples were tested for TOC, and the TOC value was distributed between 0.19 and 4.11%, with an average value of 1.73%. In general, the TOC value of marl is the lowest, ranging from 0.19 to 0.68%, followed by that of shale, ranging from 0.95 to 4.11%. The $\delta^{13}C_{org}$ values ranged from −26.84 to −24.36%, showing the characteristics of heavy carbon isotope enrichment. The results of TOC and $\delta^{13}C_{org}$ are shown in Tables 1 and 2, respectively.

4.4. Major and Trace Elements. In this study, 53 samples from well ZY1 were tested for major and trace elements. The test results are shown in Table S1. To more accurately analyze

Table 1. Results of TOC and Carbon Isotope of Kerogen Results of TOC

sample no.	depth (m)	TOC (%)	$\delta^{13}C_{org}$	sample no.	depth (m)	TOC (%)	$\delta^{13}C_{org}$
ZY1-YX-1	2668	1.02	−25.03	ZY1-YX-193	2871	0.19	−25.82
ZY1-YX-3	2688	0.95	−24.99	ZY1-8-02	2877.4	2.83	
ZY1-4-05	2699	0.94		ZY1-8-04	2879.4	3.43	
ZY1-YX-5	2702	1.46	−25.12	ZY1-8-06	2881.5	2.52	
ZY1-YX-76	2709	0.88		ZY1-8-08	2883.5	2.96	
ZY1-YX-85	2719	0.79	−24.19	ZY1-8-10	2885.5	2.45	−25.34
ZY1-YX-8	2728	1.40		ZY1-9-02	2886.5	3.34	
ZY1-YX-9	2738	1.39	−25.6	ZY1-9-04	2888.5	3.27	
ZY1-YX-11	2750	0.78	−24.72	ZY1-9-06	2890.5	2.72	−25.71
ZY1-YX-119	2759	1.12	−25.01	ZY1-9-08	2892.5	3.49	
ZY1-YX-16	2770	2.81	−25.6	ZY1-9-10	2894.4	2.81	
ZY1-YX-136	2787	2.05		ZY1-YX-32	2898	1.97	−26.03
ZY1-6-01	2796	3.90	−25.12	ZY1-YX-206	2903	0.20	
ZY1-6-03	2798.2	3.05		ZY1-YX-33	2914	0.70	
ZY1-6-05	2800.5	3.07		ZY1-YX-220	2919	0.21	−26.43
ZY1-6-07	2802.6	4.11		ZY1-YX-225	2924	0.62	
ZY1-6-09	2804.7	3.34		ZY1-10-2	2927.2	0.66	
ZY1-7-02	2807.55	3.86		ZY1-10-7	2931.95	1.25	−24.43
ZY1-7-04	2808.5	3.00		10-1	2933.48		−24.7
ZY1-7-06	2810.5	3.01		11-1	2942.75		−24.43
7-1	2811.79		−24.89	ZY1-YX-36	2938	1.31	
ZY1-7-08	2812.5	3.75	−24.92	ZY1-11-6	2944.1	0.25	−24.36
ZY1-7-10	2814.5	3.37		ZY1-12-5	2950.1	1.10	
ZY1-YX-151	2823	1.44	−25.93	ZY1-YX-234	2962	1.48	
ZY1-YX-25	2828	1.44		ZY1-YX-39	2968	0.68	
ZY1-YX-160	2834	1.81		ZY1-YX-247	2976	1.33	−26.64
ZY1-YX-26	2838	1.04	−25.59	ZY1-YX-39	2968	0.68	
ZY1-YX-172	2847	1.02		ZY1-YX-247	2976	1.33	−26.64
ZY1-YX-28	2858	1.95	−25.74	ZY1-13-1	2981.90		−26.84
ZY1-YX-186	2863	0.51					

Table 2. Calculation Results of the Element Enrichment Coefficient

	V_{EF}	Mo_{EF}	U_{EF}	Ni_{EF}	Cr_{EF}	Co_{EF}	Cu_{EF}	Zn_{EF}
min	0	0	0	0	0	0	0	0
max	6.6	4.4	2.4	3.3	1.9	0.3	1.0	1.1
average	1.1	0.9	0.5	0.7	0.8	0.1	0.3	0.4

the paleoredox conditions and paleoproductivity in the study area, this paper calculates the enrichment coefficient (X_{EF}) of eight elements that participate in the reconstruction of the paleoenvironment. The calculation results for the element enrichment coefficient are shown in Figure 10 and Table S2.

The calculation results of X_{EF} are as follows: V_{EF} ranged from 0 to 6.6 (mean 1.1); Mo_{EF} ranged from 0 to 4.4 (average 0.9); U_{EF} ranged from 0 to 2.4 (mean 0.5); Ni_{EF} ranged from 0 to 3.3 (mean 0.7); Cr_{EF} ranged from 0 to 1.9 (average 0.8); Co_{EF} ranged from 0 to 0.3 (average 0.1). Cu_{EF} ranged from 0 to 1.0 (mean 0.3). Zn_{EF} ranges from 0 to 1.1 (average 0.4). Figures 10, 11, and Supporting Materials have detailed calculation results.

To better reconstruct the palaeoenvironment of the Dawuba Formation, other parameters, such as Fe/Mn, Rb/K, CIA index, P/Al, and biological barium (Ba_{XS}), which are used to reflect the paleoproductivity and terrigenous debris input, are also calculated.

CIA ranged from 62 to 85 (mean 78), Ti/Al ranged from 0.027 to 0.067 (average 0.049), Fe/Mn ranged from 16.36 to 656.36 (average 267.41), Rb/K ranged from 1.00 to 64.42

(average 26.65), P/Al ranged from 0.12 to 3.32 (average 0.78), and Ba_{XS} ranged from −0.02 to 1.26 (average 0.20). Detailed calculation results are shown in Figures 11 and 15 and Table S2.

5. DISCUSSION

5.1. Sedimentary Model. The sedimentation model often plays a very important role in the process of organic matter enrichment. Only by establishing the sedimentation model in accordance with the study area, we can establish the organic matter enrichment model suitable for this area. Based on the interpretation results of the wide-area electromagnetic method and the analysis of the drilling and outcrop profile, the sedimentary facies zone and environment in the study area were redefined, as shown in Figure 6[51,52]

However, in the actual research process, only relying on geophysical data cannot truly reflect the sedimentary characteristics of an area. Therefore, drilling and outcrop data are generally needed to support. To establish a more accurate sedimentary model in the study area, this paper selected a total of eight Wells and outcrop across the entire platform basin for well connection analysis. The data of Huishui Xicheng section, CY-1, DY-1, and ZY_1-1 Wells were obtained from previous studies.[24,25,53,54]

From the connecting diagram of the sedimentary profile (Figure 7) in the study area, it can be seen that the thickness of the whole Dawuba Formation decreases first and then thickens from the southwest to northeast direction, and the deposition thickness of the Dawuba Formation reaches the maximum at
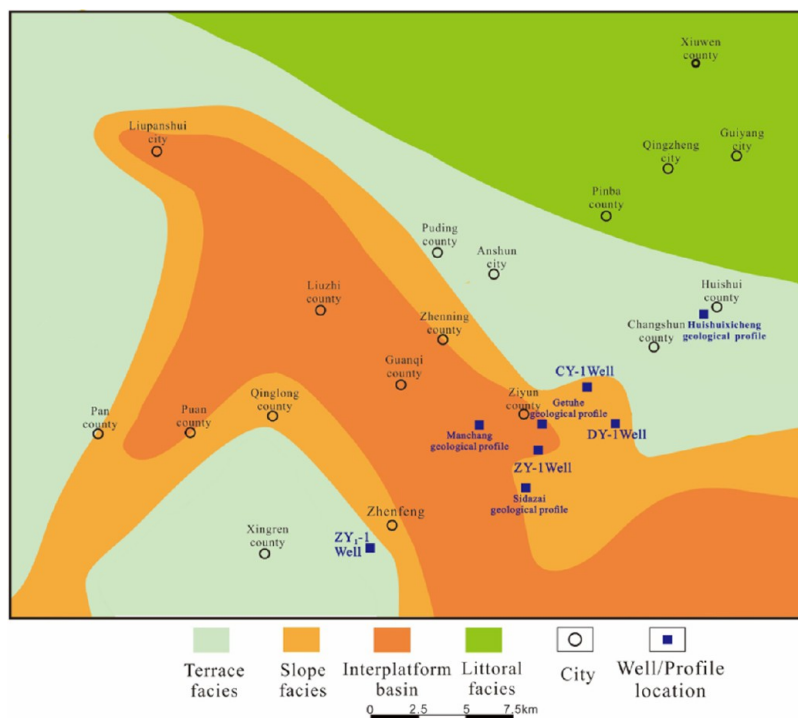
Figure 6. Map showing early Carboniferous sedimentary facies in southern Guizhou.
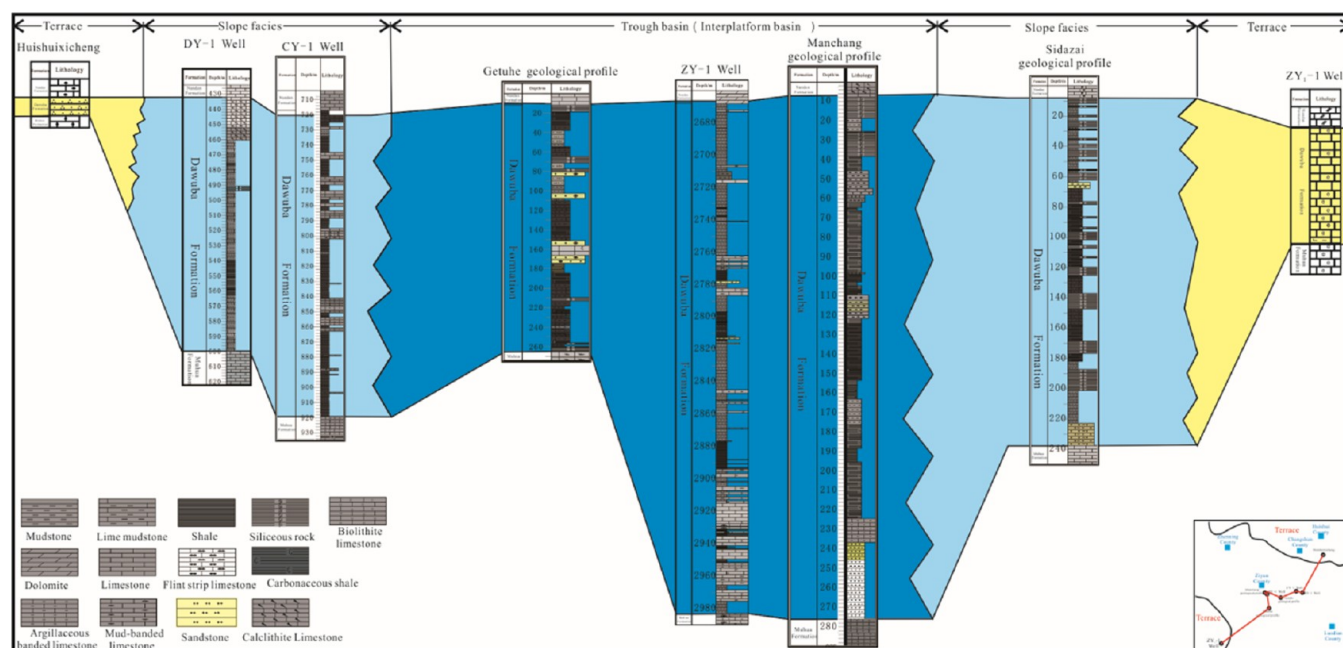

Figure 7. Sedimentary relative diagram of the Lower Carboniferous Dawuba Formation in Southern Guizhou.

Well ZY1. This is consistent with the sedimentary facies' characteristics reflected in Figure 6. At the same time, the lithology of the Dawuba Formation also changed from quartz sandstone platform facies to carbonaceous shale and carbonaceous mudstone platform basin facies, and then for ZY$_1$-1 well, it changed to carbonate platform facies again. It can be seen from the profile (Figure 7) that the paleogeographic pattern of the whole Dawuba Formation was high at both ends and low in the middle from the southwest to northeast direction.

On the basis of previous studies on geophysical exploration, the Huishui to Zhenye sedimentary model map (Figure 8) was

established by analyzing field profiles and drilling wells in the study area. In general, during the early Carboniferous Datang period, the study area experienced a seaward transgression from southwest to northwest, which basically submerged the southern and southwestern Guizhou areas, thus establishing the basic pattern of current sedimentation.[55] The sedimentary water in the whole study area deepens first and then becomes shallower from SW to NE, thus forming platform facies deposits in the Huishui area and then transferring to the continental facies denudation area dominated by clastic deposits to the north. The water body gradually deepens
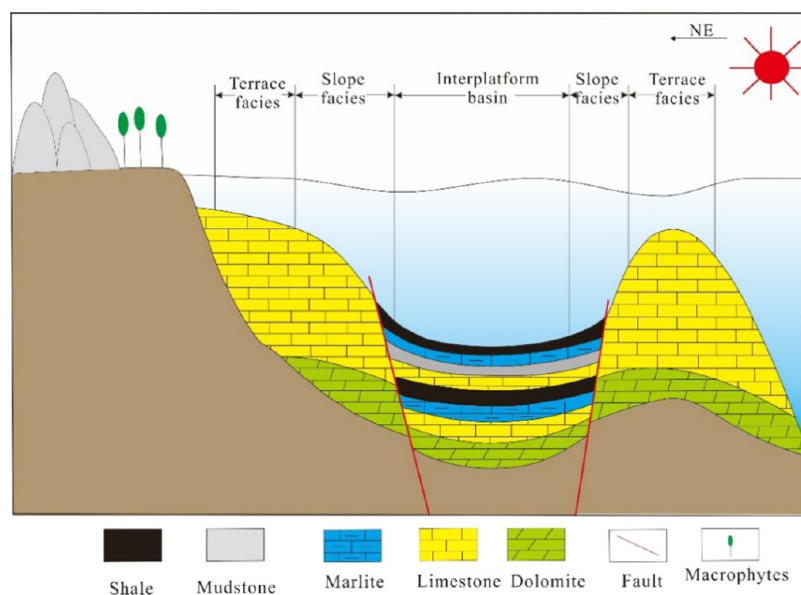
Figure 8. Sedimentary model map of Lower Carboniferous Dawuba Formation in Southern Guizhou.

toward the southwest of the study area. Therefore, the main body of the southern facies area is the platform basin facies sedimentary area, the lithology is gradually changed to limestone and shale, and the sedimentary thickness is large. In the south, the sedimentary water body gradually becomes shallow and once again transients to carbonate platform facies in the Zhenye area.

5.2. Paleoredox Conditions. A series of methods, such as U/Th, V/Cr, Ni/Co, and V/(V + Ni), have been established to distinguish the redox degree of water using the ratio of major and trace elements.[56−60] However, with the deepening of the follow-up study, many geologists have found that only the pure element ratio to reflect the water redox environment is controlled by a particular sedimentary environment and is not widely used. And with a fixed threshold to distinguish between water redox environment and not in combination with the sedimentary background also tend to appear limitations.[61,62] More importantly, Algeo and Liu concluded that the use of element enrichment coefficients can more accurately reflect the characteristics of the oxygen content in water bodies.[62] On the basis of previous studies, five elements, V, Mo, U, Co, and Cr, which can better reflect the redox conditions of water during the sedimentation process, were selected to judge the redox conditions of water during shale deposition in the study area according to the characteristics of chemical changes of different elements under different oxygen conditions.[63−70] Based on the above characteristics, five redox-sensitive elements, Mo, U, V, Cr, and Co, were selected in this paper to reconstruct the paleoredox environment of Dawuba Formation. To exclude the influence of terrigenous input on the experimental results. In this paper, the average element content (AUC) in the upper crust was used as the standard to calculate the enrichment index of the above four elements. The calculation results are shown in Figure 10, and the detailed data and value range of corresponding parameters are shown in Tables S2 and 2.

The results indicate that the enrichment coefficients of RSTEs show the characteristics of fluctuation in the whole Dawuba Formation. This feature is due to the presence of carbonate rocks in the selected samples, so X_{EF} of the X

section, which mainly develops limestone, is higher than that of the shale section. This characteristic of carbonate rock is caused by the depth of its sedimentary water. However, the enrichment coefficients of RSTEs are all less than 1 in the S section of shale, and only a few data points are slightly higher than 1. On this basis, it can be observed that the enrichment coefficient of RSTEs shows two obvious low-value regions, indicating that the sedimentary water body of the Dawuba Formation should have experienced a relatively oxygen-rich period in these two low-value regions. In general, the enrichment coefficients of RSTEs in the whole mud shale of the Dawuba Formation are all less than 1, indicating that the mud shale of the Dawuba Formation occurs in an oxidized/suboxidized sedimentary environment, and the occurrence of the low-value area indicates that the mud shale of the Dawuba Formation may have experienced two oxygen-rich periods. In addition to using the enrichment coefficient of RSTEs to distinguish the depositional environment of the Dawuba Formation, this paper also uses the Mo−U covariant diagram to further distinguish the oxidation environment of the Dawuba Formation during the depositional period. According to the Mo−U covariation diagram (Figure 9), all of the data points of the whole Dawuba Formation fall in the range of oxidation/suboxidation, which is consistent with the characteristics of the enrichment coefficient of RSTEs. The above characteristics indicate that there was sufficient oxygen in water during the shale deposition period of the Dawuba Formation, which may be conducive to the growth of marine microorganisms but is not conducive to the preservation and accumulation of organic matter in the long term (Figure 10).

5.3. Paleoproductivity. The accumulation of organic matter in sediments is not only controlled by water redox conditions but also closely related to primary productivity.[5] Therefore, it is of great significance to evaluate the paleoproductivity in an area for understanding the enrichment degree and mode of organic matter in this area. To objectively and accurately evaluate the paleoproductivity of a region, the paleoproductivity index is generally used to evaluate it. According to previous studies, TOC, P/Al, Ni_{EF}, Ba_{XS}, Cu_{EF}, and Zn_{EF} are generally selected as indicators of paleoproduc-
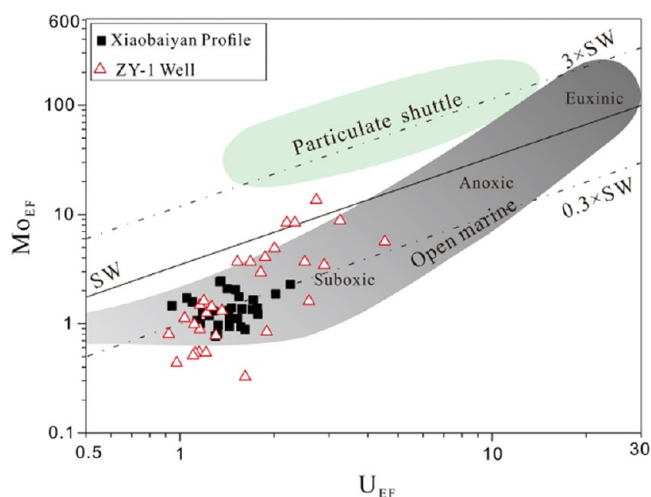
Figure 9. Cross plot of U_{EF} vs Mo_{EF} shows the majority of samples from the entire ZY1 well in the oxidized/suboxidized range. The data from the Xiaobaiyan profile are from Ding's study,[71] which was also conducted in the same area.

tivity in the study area.[63,72] TOC, which is directly related to the organic matter in the deposition process, is the most direct and important index to study paleoproductivity. As nutrient elements, Zn, Cu, Ni, and P are directly involved in the biological cycle of algae and plankton. Therefore, the enrichment degree of these elements in water can also reflect the growth of algae and plankton in water during the same period.[63,73,74] Although Ba does not directly participate in the biological cycle of algae and plankton, Ba can only be preserved in the deposition process by combining with SO_4^{2-} generated by algae metabolism. Therefore, Ba can also be used as a reflection of the algae prosperity in the water body during the deposition period.[75,76] However, due to the complexity of the deposition process, normalized parameters such as P/Al, Ni_{EF}, Ba_{XS}, Cu_{EF}, and Zn_{EF} are usually used to correct the content of each element to eliminate other influences.

The details of paleoproductivity indicators are shown in Table S2 and Figure 11, and the range of parameter values is shown in Table 2. In terms of the variation characteristics, both the paleoproductivity index and the paleoredox index of the Dawuba Formation fluctuate up and down. The paleoproductivity index of section X is relatively higher than that of section S, and almost all of the samples with high paleoproductivity indexes are carbonate rocks. According to previous studies, the lower limestone of the Dawuba Formation is mainly bioclastic limestone.[23,25] This result indicates that the limestone samples in this study generally show the characteristics of high paleoproductivity. However, the enrichment coefficients of Zn, Cu, and Ni are all less than 1 in the S section of the shale, and the values of only a few samples are greater than 1, indicating that there were not enough nutrient elements to supply the growth and development of paleontology in the seawater during this period. In addition, the average P/Al of all samples in the study area is only 0.008, and the average P/Al of shale samples is only 0.006, while the ratio of the two is 0.011 in the AUCC. This indicates that P is an element that constitutes the biological skeleton, and the content in the mud shale in the study area is low. It also indicates that there is not enough P element to supply plankton in the deposition in the study area. Finally, although the value of Ba_{XS}, which is closely related to biological

activities, is relatively lower in the upper shale section than in the lower limestone segment, the value of this parameter is still relatively low on the whole, and a considerable number of samples have negative values. All of these characteristics indicate that biological activities are not frequent in the Dawuba Formation. However, TOC, which can directly reflect the enrichment degree of organic matter, shows the characteristics of contradiction with the above parameters. The TOC value of the upper part of shale is higher than that of the lower part of limestone, and there are two high TOC values in the lower part of productivity. It can be seen from Figure 12 that TOC shows a negative correlation with the productivity indices Ba and P/Al, and the correlation between TOC and the two productivity indices is not high. These characteristics are contradictory to the conclusion of low paleoproductivity in the Dawuba Formation, indicating that other factors may have dominated the enrichment of organic matter during the development of mud shale in the Dawuba Formation.

5.4. Terrestrial Input. The terrigenous detrital input always exists in the sedimentation process, and the material with terrigenous detrital entering the sedimentary stratum will play a direct role in the accumulation of organic matter in the stratum. Previous studies indicate that the Lower Carboniferous Dawuba Formation is located in a slope facies sedimentary environment with frequent terrigenous input.[71] In addition, previous studies on the profile of the Dawuba Formation have found that the interbedded sandstone beds have positive grain sequences and the abrupt contact between different lithologies can be seen in some locations of the profile. All of these pieces of evidence indicate that there may be a typical phenomenon of debris input in the dam formation, namely, the existence of gravity flow.[73] In this study, the characteristics of terrigenous detrital input in the Dawuba Formation were analyzed by logging data, core observation, field profile deposition characteristics, microscopic thin section observation, and major and trace elements' characteristics.

First, argillaceous nodules prevalent in the field section, abrupt contact between sandstone and surrounding rock. The presence of quartz clots and terrigenous debris in mudstone observed in microscopic thin sections is also evidence of strong terrigenous input in the Dawuba Formation (Figures 2−4). In addition, previous studies have pointed out that, in general, the development of gravity flow tends to occur in areas with large terrigenous input.[77] So, the development of gravity flow can be regarded as an indication that a region experienced terrigenous input during a certain sedimentary period. Whether gravity flow is developed in the formation needs to be judged by the profile characteristics and drilling core characteristics in this area. A series of sedimentary characteristics, such as wavy bedding, massive bedding, clastic bedding, and coiling bedding, can be observed in the cores of the strata developed by gravity flow.[77] In addition, some studies have shown that natural gamma-ray (GR) logs exhibited unique box characteristics, which can also be used to judge whether gravity flow is developed in the formation.[77,78] Through the analysis of the Well ZY1 logging curve, it can be observed that in the depth range of the abnormally low paleoredox and paleoproductivity data mentioned in the previous article, the corresponding GR logging curve also shows box characteristics. Meanwhile, in the same depth range, wavy bedding, sand/limestone masses, rolled bedding, and clastic deposits can be observed on the cores, which can reflect the development of gravity flow. Core
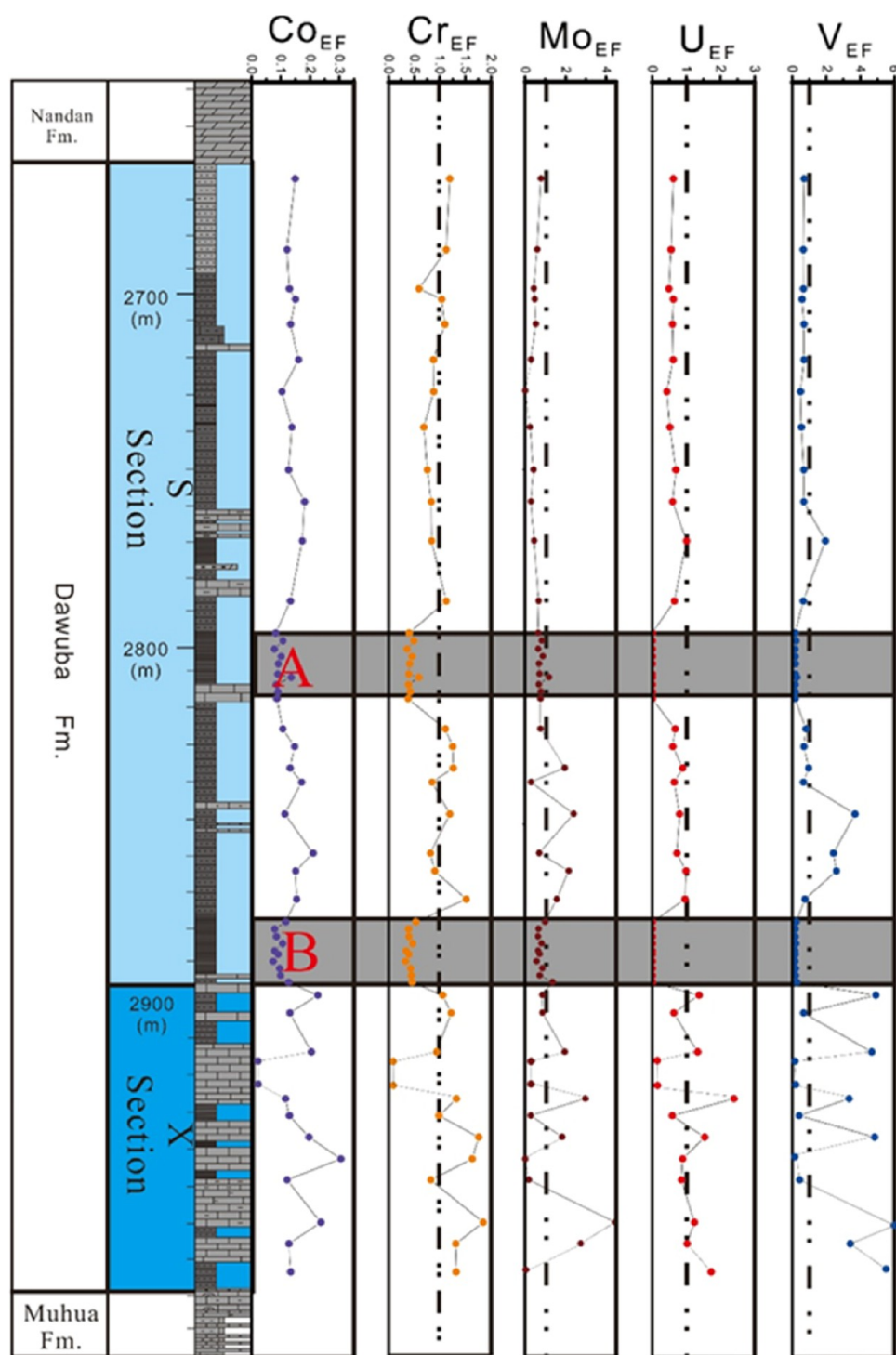
Figure 10. Chemostratigraphic profiles of redox proxies for the ZY1 well. In the dark areas, the element enrichment coefficient decreased significantly.

characteristics and logging curve characteristics are shown in Figure 13.

In addition, element geochemical data analysis is also used to further analyze the terrigenous input characteristics of the Dawuba Formation. In this study, chemical weathering index (CIA), terrestrial detrital index (Ti/Al), Fe/Mn, and Rb/K, which are used to reflect changes of water depth, were selected for analysis and explanation. Previous studies have pointed out that Fe/Mn ratio tends to increase as the water depth becomes shallower, while the Rb element can migrate to a long distance

because it is easy to be adsorbed by clay minerals, so the Rb/K value will decrease as the water depth becomes shallower.[79,80] By combining these two parameters, which are completely opposite with the change of water depth, the changes of water depth in different sedimentary periods can be more accurately obtained. The chemical weathering index (CIA) is used to reflect the degree of weathering of rocks. When the chemical weathering index (CIA) value becomes higher, more detrital material will be generated, which provides sufficient material conditions for terrigenous input. Finally, Ti and Al, as the main
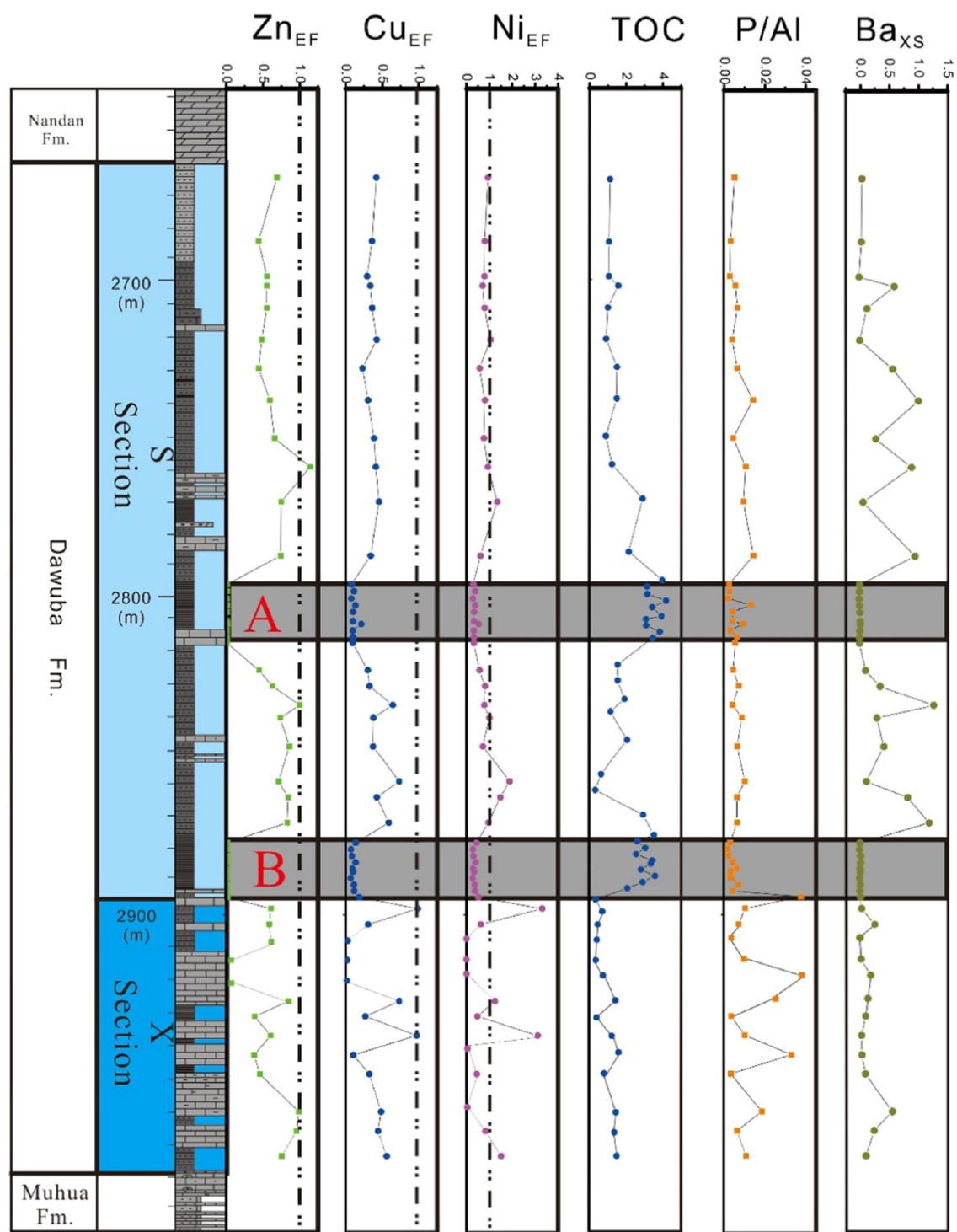
Figure 11. Chemostratigraphic profiles of paleoproductivity for the ZY1 well. In the dark areas are the water depth change section and TOC high-value section.

elements in the crust, tend to migrate into seawater in the geological process, among which Al participates in the formation of feldspar and clay minerals, while Ti forms a series of terrigenous heavy minerals, such as pyroxene with strong stability. Therefore, the input of terrigenous debris in the ocean can be expressed as Ti/Al. The higher the Ti/Al ratio, the greater the terrigenous input in this period.[81,82]

Meanwhile, the average value of CIA in the upper S section was 79.24, while that in the lower X section was 75.83. The value of the upper S section is higher than that of the lower X

section. In addition, it can be seen from Figure 16 that the samples in the study area are in the moderately strong weathering zone. This indicates that the degree of weathering was higher during the mudstone deposition period, which provided conditions for the importation of terrigenous debris. At the same time, there are two high values of CIA in the S section, indicating that the chemical weathering degree reached the maximum and the clastic provenance was the most abundant in this period. Coincidentally, the depth of the relatively high CIA value area corresponds to the location
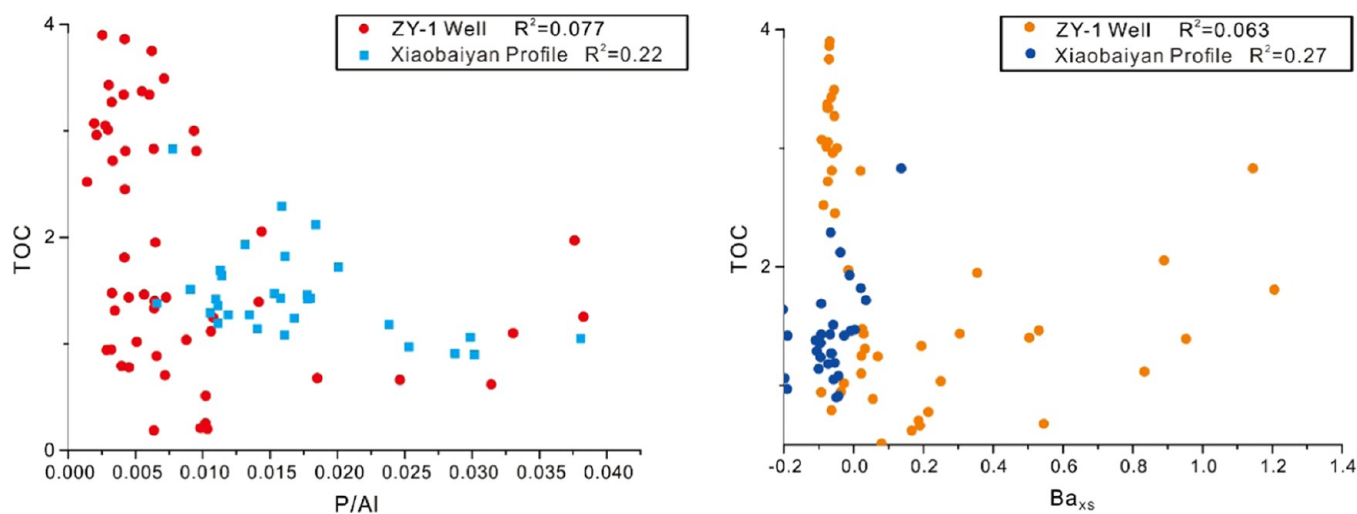
Figure 12. Chemostratigraphic profiles of paleoproductivity for the ZY1 well. In the dark areas are the water depth change section and TOC high-value section. The data from the Xiaobaiyan profile are from Ding's study,[71] which was also conducted in the same area.

Figure 13. Image of cores from the presumed gravity section of the ZY1 well. (A) ripple bedding, (B) sand colt, (C) oblique ripple bedding, (D) gray colt, (E) limestone debris and convolute bedding, (F) sandstone−mudstone interbed and limestone debris, and logging curve of DWB Formation; the GR curve between red line segments is box segment. The GR log is box-shaped and can indicate the presence of gravity flow.

where gravity is presumed to have developed. A relatively high level of CIA can provide a material basis for the development of gravity flow. The Ti/Al value has no obvious fluctuation compared with the CIA value, but the overall value is at a relatively high level. There is an increase in the depth segment where the CIA value is high, but this upward trend is not obvious.

The two parameters of CIA and Ti/Al (the value range of CIA and Ti/Al is shown in Table 3) indicate that the whole Dawuba Formation shale has sufficient detrital material in the deposition process. It also shows that the Dawuba formation is

Table 3. Calculation Results of Palaeoproductivity and Terrigenous Input index

	CIA	Ti/Al	Fe/Mn	Rb/K	P/Al	Ba$_{XS}$
min	62	0.025	0	1.00	0.001	−0.09
max	85	0.062	722.00	64.42	0.038	1.21
average	78	0.045	288.60	26.65	0.474	0.15

affected by terrigenous detrital input to varying degrees, and the two parameters have relatively high values in the two depth ranges of assumed gravity flow development. In addition, to more accurately reflect the terrigenous input of the study area, this paper collected the data of major elements from the Lower Carboniferous shale in Canada and compared them with the study area.[83−85] Figure 14 shows that the sedimentation rate of the study area is almost the same as that of Canada's Big Marsh area and the terrigenous input of shale is similar to that of Canada's Albert area. Due to the high sedimentation rate and terrigenous input of the Albert area in the Big Marsh area of Canada, similar element characteristics suggest that the shales in the study area may also be in a high sedimentation rate and terrigenous input environment (Figures 15 and 16).

The Fe/Mn and Rb/K parameters reflecting the variation of the water depth have a similar trend to other geochemical parameters. At the same depth, there are two high-value segments of Fe/Mn and two obvious low-value segments of Rb/K, which indicates that the depth of the sedimentary water
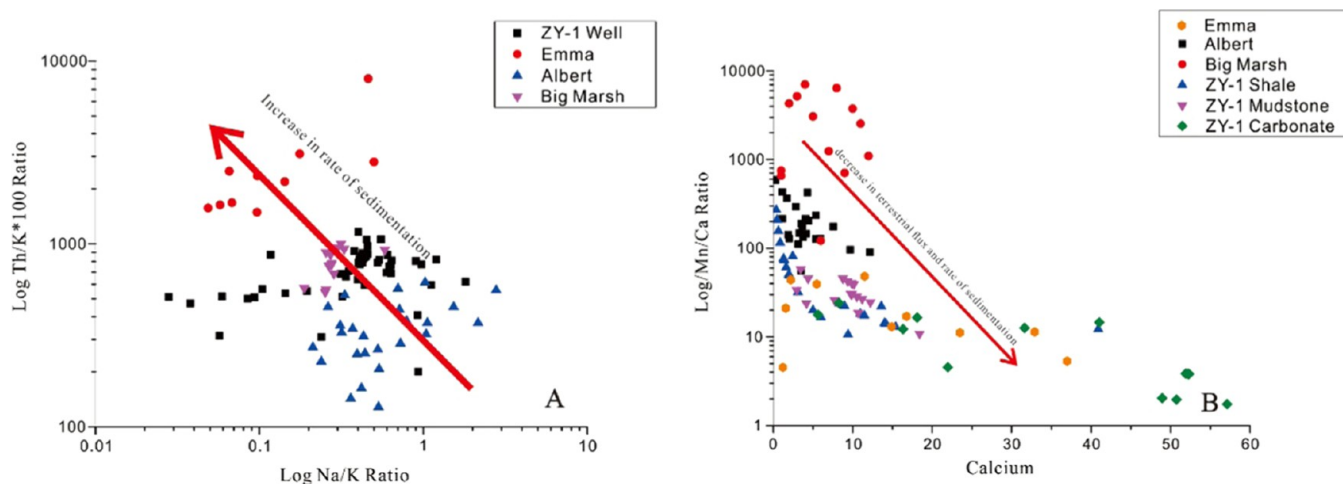
Figure 14. (A) Rate of sedimentation for Big Marsh, Albert, Emma Fiord, and ZY1 well oil shale based on Th/K−Na/K ratios. (B) Rate of terrestrial flux for oil shales for Big Marsh, Albert, Emma Fiord, and ZY1 well oil shale based on Th/K−Na/K ratios.

body of the Dawuba Formation has changed significantly at these two depths. However, due to the relatively stable sedimentary environment of the whole Dawuba, there will not be a large change of water depth in a short time. Therefore, the change of Fe/Mn and Rb/K values is due to the influence of terrigenous debris. All of these characteristics indicate that the shale of the Dawuba Formation received terrigenous material input continuously during the deposition process, and terrigenous debris input reached the maximum in the two depth segments where gravity flow is supposed to develop.

5.5. Models of Organic Matter Accumulation. Previous studies pointed out that the accumulation of organic matter in strata usually goes through three processes: generation, destruction (preservation), and dilution.[87] Moreover, only the organic matter particles that have experienced all three processes can remain in the formation and form oil and gas in the later diagenetic process.[87] These three processes correspond to paleo-productive conditions, paleoredox conditions, and terrigenous detritus input, respectively.[20]

Based on the sedimentary model established above, it is clear that the shale of the Dawuba Formation belongs to platform basin facies, and the NE direction of the study area is close to the ancient land of the Upper Yangtze. In addition, the paleoredox environment, paleoproductivity conditions, and terrigenous debris importation of the Dawuba Formation shale have been analyzed previously. On this basis, it is clear that the mud shale of the Dawuba Formation developed in an oxidized/suboxidized and low-productivity sedimentary environment, and at the same time, it was diluted by terrigenous detrital inputs during the whole sedimentary period of the mud shale. From these conditions, the whole Dawuba formation is not conducive to the enrichment of organic matter in the stratum. However, it can be seen from the TOC test data that the TOC value appears high in the upper S segment of Dawuba shale development, there are two obvious high-value segments between the depths of 2896−2814 and 2877−2894 m, and the TOC value of the high-value segment is about 3.0%. The TOC value of some samples can reach around 4.0%. This indicates that there is a large amount of organic matter enrichment in the Dawuba Formation. At the same time, the depth at which TOC values appear coincidentally corresponds to the period when the oxygen content is the highest and paleoproductivity is the lowest in the sedimentary water of the

Dawuba Formation. These contradictory results indicate that the enrichment of organic matter in the mud shale of the Dawuba Formation is not completely controlled by productivity conditions and preservation conditions. However, coincidentally, the high value of TOC coincides with the period when terrigenous input is the most intense in the Dawuba Formation, so it is speculated that terrigenous input may increase the organic matter content in the Dawuba Formation shale. To show that the terrigenous detrital input increased the organic matter content in the Dawuba shale, it is necessary to show that the terrigenous detrital material carried sufficient organic matter during the transport process. Combined with the filamentous organic matter observed by SEM photos of the Dawuba Formation (Figure 5A,C,I), it can be concluded that there is higher plant debris in the Dawuba mud shale. Additionally, the carbon 13 isotope ($\delta^{13}C_{org}$) of kerogen ranges from −26.84 to −24.36%, which belongs to the isotopic characteristics of terrestrial C3 plants, indicating that there are indeed a large number of higher terrestrial plant components in the Dawuba shale. Therefore, it is proved that the terrigenous input that existed continuously during the deposition period of the Dawuba Formation not only brought inorganic detrital in the shallow part but also carried a large amount of organic detrital. This sedimentary feature makes up for the defects of shale preservation and production and increases the organic matter content of the shale in the Dawuba Formation.

Overall, the Dawuba Formation of mud shale was deposited in a period of relatively rich oxygen. During this period, although enough oxygen for algae in the water body and the breeding of microorganisms provide the condition, the effect of water to support microbial multiply the lack of elements are limiting the number of microorganisms, thereby resulting in the water during this period the low paleoproductivity. Under the condition of low paleoproductivity, the high oxygen content of water further increases the difficulty of organic matter preservation. However, in the deposition process of the Dawuba Formation, the higher plant debris with terrigenous input into the stratum made up for the defects of the preservation conditions and productivity during the deposition period and increased the content of organic matter in the shale of the Dawuba Formation. Therefore, the Dawuba Formation formed a set of organic matter accumulation modes dominated
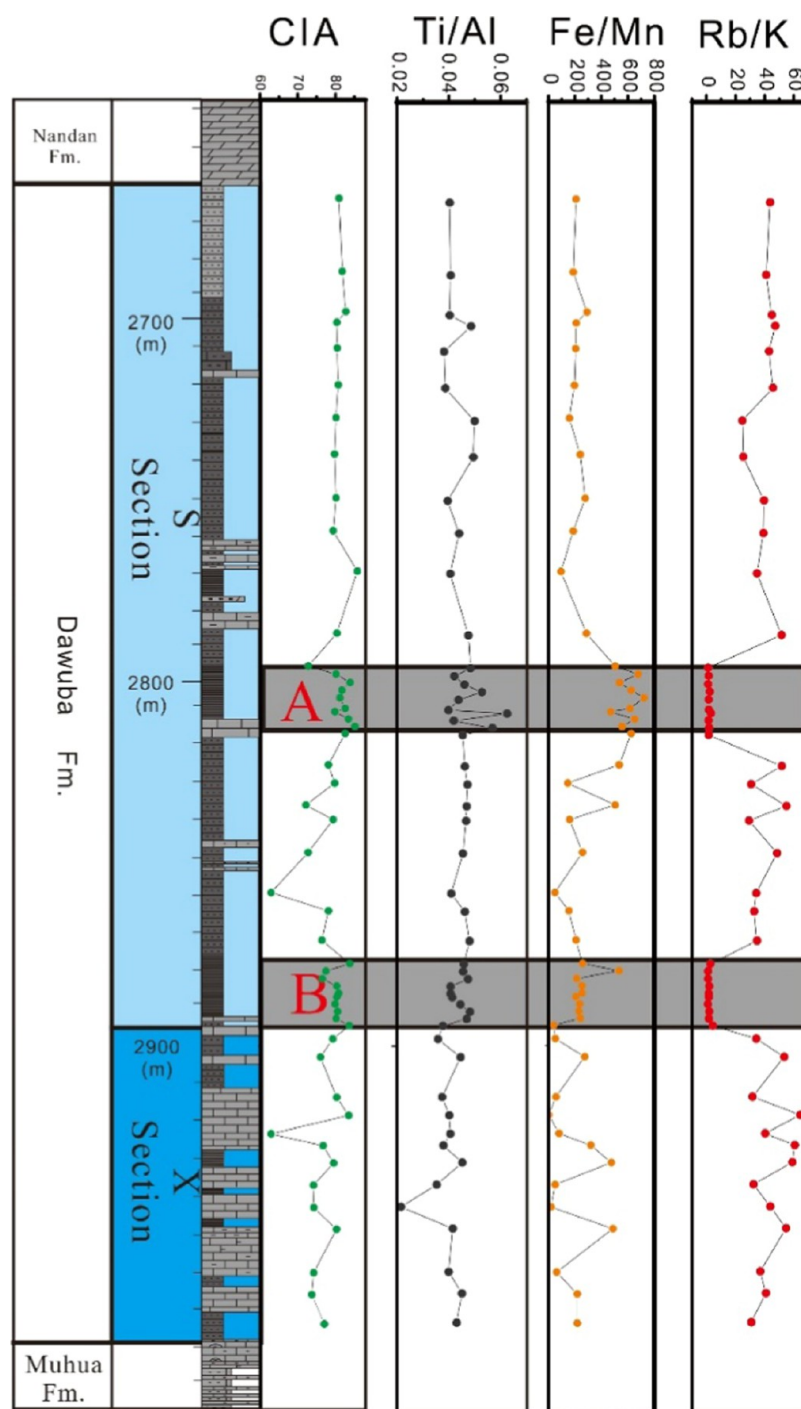
Figure 15. Chemostratigraphic profiles of terrigenous input and water depth for the ZY1 well. In the dark areas are the high-value area of terrigenous detrital input and the abnormal area of water depth change.

by terrigenous organic matter under the condition of high oxygen content and low water productivity (Figure 17).

6. CONCLUSIONS

(1) Both the enrichment coefficient of redox-sensitive elements and the $Mo_{EF}-U_{EF}$ covariant index indicate that the shale of the Dawuba Formation was deposited in an oxygen-rich water body. Under oxygen-rich conditions, it is favorable for the development of plankton in the ocean. However, under oxygen-rich conditions, the microbial remains in the water will be

difficult to be preserved in the sediments, which leads to difficulty in the preservation of organic matter in the strata of the Dawuba Formation.

(2) The paleoproductivity index of the Dawuba Formation indicates that the primary productivity of the Dawuba Formation is at a low level during the sedimentary period. Although the oxygen-rich water provides favorable conditions for the growth of plankton, the lack of nutrient elements in the water restricts microbial reproduction to some extent. However, the abnormally high TOC value in the Dawuba shale indicates that
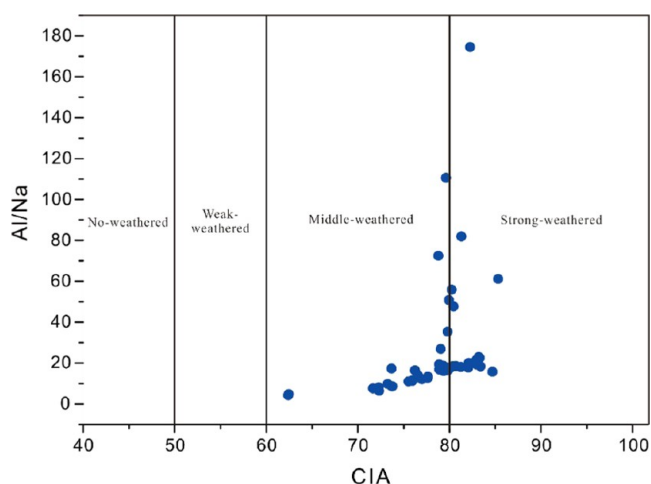
Figure 16. Cross plot of CIA values versus Al/Na ratios demonstrating the weathering degree in the ZY1 well (the plate after[86]).
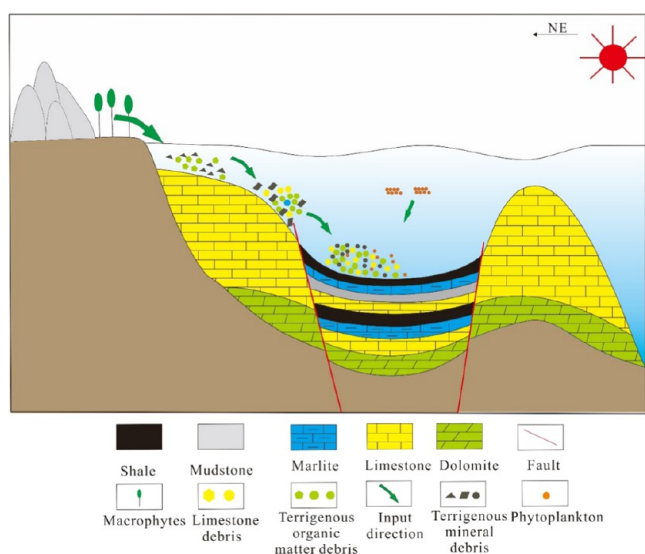

Figure 17. Organic matter enrichment pattern of Lower Carboniferous DWB Formation in Qiannan Depression; the polygon of the same color in the figure represents the rounding of the same kind of debris in the process of transport and deposition.

although the shale of the Dawuba Formation is in a sedimentary period of low paleoproductivity, it still maintains the characteristic of high TOC value under the influence of other factors.

(3) The parameters reflecting the terrigenous debris input indicate that the shale of the Dawuba Formation was continuously affected by terrigenous debris input during the deposition period. Meanwhile, according to the core observation and logging characteristics, two strong terrigenous inputs occurred at the depths of 2796−2814 and 2877−2894 m, which also represent the gravity flow deposition.

(4) From the perspective of paleoproductivity level and water redox, the Dawuba Formation is not conducive to the generation and preservation of organic matter. Paradoxically, the high TOC interval of the Dawuba Formation shale happens to be at the depth where the water is most oxygen-rich and the productivity is least.

This evidence suggests that the characteristics of high TOC in the Dawuba Formation shale may not be completely controlled by production and preservation conditions. At the same time, the depth at which the gravity flow develops also corresponds to the high-value region of TOC. According to the scanning electron microscopy (EE-SEM) photos and the kerogen carbon isotope 13 ($\delta^{13}C_{org}$) results, there is a large amount of terrigenous organic matter in the shale of the Dawuba Formation that enters the sedimentary strata with terrigenous detrital. The existence of these terrigenous organic matter makes up for the defects of poor productivity and preservation conditions and is also evidence that the accumulation of organic matter in the Dawuba Formation is dominated by terrigenous detrital. Therefore, the shale of the Dawuba Formation formed an organic matter accumulation mode dominated by terrigenous organic matter in the water body with high oxygen content and low productivity.

■ ASSOCIATED CONTENT

Ⓢ Supporting Information

The Supporting Information is available free of charge at https://pubs.acs.org/doi/10.1021/acsomega.1c03809.

Elemental geochemical data and TOC data (PDF)

■ AUTHOR INFORMATION

Corresponding Authors

Jinchuan Zhang − School of Energy Resources, China University of Geosciences, Beijing 100083, China; Key Laboratory of Strategy Evaluation for Shale Gas of Ministry of Land and Resources, China University of Geosciences, Beijing 100083, China; ⊙ orcid.org/0000-0002-2979-4866; Email: zhangjc@cugb.edu.cn

Xuan Tang − School of Energy Resources, China University of Geosciences, Beijing 100083, China; Key Laboratory of Strategy Evaluation for Shale Gas of Ministry of Land and Resources, China University of Geosciences, Beijing 100083, China; State Key Laboratory of Shale Oil and Gas Enrichment Mechanisms and Effective Development, Beijing 100083, China; ⊙ orcid.org/0000-0002-6074-9633; Email: tangxuan@cugb.edu.cn

Authors

Jialiang Niu − School of Energy Resources, China University of Geosciences, Beijing 100083, China; Key Laboratory of Strategy Evaluation for Shale Gas of Ministry of Land and Resources, China University of Geosciences, Beijing 100083, China

Kun Yuan − School of Energy Resources, China University of Geosciences, Beijing 100083, China; Oil and Gas Survey Center, China Geological Survey, Beijing 100083, China

Tuo Lin − Oil and Gas Survey Center, China Geological Survey, Beijing 100083, China

Yang Liu − School of Energy Resources, China University of Geosciences, Beijing 100083, China; Key Laboratory of Strategy Evaluation for Shale Gas of Ministry of Land and Resources, China University of Geosciences, Beijing 100083, China

Yanjie Niu − Gansu Coalfield Geology Bureau 145th Team Exploration Engineering Company, Zhangye City 734000, China

Pei Li − *School of Energy Resources, China University of Geosciences, Beijing 100083, China; Petroleum Exploration and Production Research Institute, China Petroleum and Chemical Corporation (SINOPEC), Beijing 100083, China;* ⊙ orcid.org/0000-0002-2470-6185

Xingqi Li − *School of Energy Resources, China University of Geosciences, Beijing 100083, China; Key Laboratory of Strategy Evaluation for Shale Gas of Ministry of Land and Resources, China University of Geosciences, Beijing 100083, China*

Yutao Liang − *School of Energy Resources, China University of Geosciences, Beijing 100083, China; Key Laboratory of Strategy Evaluation for Shale Gas of Ministry of Land and Resources, China University of Geosciences, Beijing 100083, China*

Complete contact information is available at:
https://pubs.acs.org/10.1021/acsomega.1c03809

Notes
The authors declare no competing financial interest.

■ REFERENCES

(1) Arthur, M. A.; Sageman, B. B. Marine black shales: depositional mechanisms and environments of ancient deposits. *Annu. Rev. Earth Planet. Sci.* **1994**, *22*, 499−551.

(2) Burdige, D. J. Preservation of organic matter in marine sediments: controls, mechanisms, and an imbalance in sediment organic carbon budgets? *Chem. Rev.* **2007**, *107*, 467−485.

(3) Li, C.; Jin, C.; Planavsky, N. J.; Algeo, T. J.; Cheng, M.; Yang, Y.; Zhao, Z.; Xie, X. Coupled oceanic oxygenation and metazoan diversification during the early-middle Cambrian? *Geology* **2017**, *45*, 743−746.

(4) Mort, H.; Jacquat, O.; Adatte, T.; Steinmann, P.; Föllmi, K.; Matera, V.; Berner, Z.; Stüben, D. The Cenomanian/Turonian anoxic event at the Bonarelli Level in Italy and Spain: enhanced productivity and/or better preservation? *Cretaceous Res.* **2007**, *28*, 597−612.

(5) Pedersen, T. F.; Calvert, S. E. Anoxia vs. productivity: what controls the formation of organic-carbon-rich sediments and sedimentary rocks? *AAPG Bull.* **1990**, *74*, 454−466.

(6) Sageman, B. B.; Murphy, A. E.; Werne, J. P.; Ver Straeten, C. A.; Hollander, D. J.; Lyons, T. W. A tale of shales: the relative roles of production, decomposition, and dilution in the accumulation of organic-rich strata, Middle−Upper Devonian, Appalachian basin. *Chem. Geol.* **2003**, *195*, 229−273.

(7) Wang, X.; Zhu, Y.; Lash, G. G.; Wang, Y. Multi-proxy analysis of organic matter accumulation in the Upper Ordovician−Lower Silurian black shale on the Upper Yangtze Platform, south China. *Mar. Pet. Geol.* **2019**, *103*, 473−484.

(8) Dang, W.; Jiang, S.; Zhang, J.; Li, P.; Nie, H.; Liu, Y.; Li, F.; Sun, J.; Tao, J.; Shan, C.; Tang, X.; Wang, R.; Yin, Y. A systematic experimental and modeling study of water adsorption/desorption behavior in organic-rich shale with different particle sizes. *Chem. Eng. J.* **2021**, *426*, No. 130596.

(9) Jinchuan, Z.; Zhijun, J.; Mingsheng, Y. Reservoiring mechanism of shale gas and its distribution. *Nat. Gas Ind.* **2004**, *24*, 15−18.

(10) Li, Y.; Wang, Z.; Gan, Q.; Niu, X.; Xu, W. Paleoenvironmental conditions and organic matter accumulation in Upper Paleozoic organic-rich rocks in the east margin of the Ordos Basin, China. *Fuel* **2019**, *252*, 172−187.

(11) Tyson, R. V. The″ productivity versus preservation″ controversy: cause, flaws, and resolution. *Special Publication-SEPM*; 2005, *82*, 17.

(12) Kumar, S. P.; Ramaiah, N.; Gauns, M.; Sarma, V.; Muraleedharan, P. M.; Raghukumar, S.; Kumar, M. D.; Madhupratap, M. Physical forcing of biological productivity in the Northern Arabian Sea during the Northeast Monsoon. *Deep Sea Res., Part II* **2001**, *48*, 1115−1126.

(13) Canfield, D. E. Factors influencing organic carbon preservation in marine sediments. *Chem. Geol.* **1994**, *114*, 315−329.

(14) Calvert, S. E.; Karlin, R. E.; Toolin, L. J.; Donahue, D. J.; Southon, J. R.; Vogel, J. S. Low organic carbon accumulation rates in Black Sea sediments. *Nature* **1991**, *350*, 692−695.

(15) Demaison, G. J.; Moore, G. T. Anoxic environments and oil source bed genesis. *AAPG Bull.* **1980**, *64*, 1179−1209.

(16) Wei, H.; Chen, D.; Wang, J.; Yu, H.; Tucker, M. E. Organic accumulation in the lower Chihsia Formation (Middle Permian) of South China: constraints from pyrite morphology and multiple geochemical proxies. *Palaeogeogr., Palaeoclimatol., Palaeoecol.* **2012**, *353−355*, 73−86.

(17) Li, Y.; Zhang, T.; Ellis, G. S.; Shao, D. Depositional environment and organic matter accumulation of Upper Ordovician−Lower Silurian marine shale in the Upper Yangtze Platform, South China. *Palaeogeogr., Palaeoclimatol., Palaeoecol.* **2017**, *466*, 252−264.

(18) Xu, X.-T.; Shao, L.-Y.; Eriksson, K. A.; Pang, B.; Wang, S.; Yang, C.-X.; Hou, H.-H. Terrestrial records of the early Albian Ocean Anoxic Event: Evidence from the Fuxin lacustrine basin, NE China. *Geosci. Front.* **2022**, *13*, No. 101275.

(19) Mei, M. X.; Yong-Sheng, M. A.; Deng, J.; Chu, H. M.; Liu, Z. R.; Zhang, H. Carboniferous to Permian sequence stratigraphic framework of the Yunnan-Guizhou-Guangxi basin and its adjacent areas and global correlation of third-order sea-level change. *Geol. China* **2005**, *32*, 13−24.

(20) Tian, Y.; Cao, Y.; Wang, Y.; Zhang, S. Sediment Dynamics Process and Sedimentary Characteristics of Hyperpycnal Flows. *Geol. Rev.* **2015**, *61*, 23−33.

(21) Yang, R.; Chen, W.; Zhou, R. Characteristics of Organic-rich Shale and Exploration Area of Shale Gas in Guizhou Province. *Nat. Gas Geosci.* **2012**, *23*, 340−347.

(22) Chen, R.; Kung, Y.; Ziya, Z.; Qiufeng, X.; Shufan, L.; Jinbo, H. Geochemical characteristics and significance of organic-rich shales in the Dawuba Formation, western Guizhou. *Pet. Geol. Exp.* **2019**, *41*, 10−15.

(23) He, B. *Sedimentary Environment of Lower Carboniferous Dawuba Formation in Ziyun Area*; Guizhou Province. Guizhou University, 2019.

(24) Lu, S.; He, B.; Du, S. Geological conditions and exploration prospect of shale gas in Dawuba Formation of Lower Carboniferous of Daiye-1 well in southern Guizhou Province. *Prov., Geol. Cond. Explor.* **2016**, *3*, 6−11.

(25) Su, H. *Analysis of sedimentary environment and hydrocarbon source rock characteristics of black shale of Carboniferous Dawuba Formation in Hui underwater*; Guizhou University: Guizhou Province, 2018.

(26) Yuan, K.; Wang, C.; Qin, Y.; Yu, S.; Zhou, Z. The discovery of Carboniferous shale gas in Qianziye-1 well of Qianan (southern Guizhou) depression). *Geol. China* **2017**, *44*, 1253−1254.

(27) Yuan, K.; Chen, R.; Lin, T.; Fang, X.; Qin, Y.; Wang, C.; Zhou, Z.; Sun, X.; Amp, O.; Center, G. S. Petrological characteristics and sedimentary environment in the southern Guizhou during the Late Carboniferous. *Pet. Geol. Exp.* **2019**, *41*, 38−44.

(28) Liang, D.; Guo, T.; Chen, J.; Bian, L.; Zhe, Z. Some Progresses on Studies of Hydrocarbon Generation and Accumulation in Marine Sedimentary Regions, Southern China (Part 2):Geochemical Characteristics of Four Suits of Regional Marine Source Rocks, South China. *Mar. Origin Pet. Geol.* **2009**, *14*, 1−15.

(29) Pan, J. P.; Qiao, D. W.; Shi-Zhen, L. I.; Zhou, D. S.; Lin-Feng, X. U.; Zhang, M. Y. Shale-gas geological conditions and exploration

prospect of the Paleozoic marine strata in lower Yangtze area, China. *Geol. Bull. China* **2011**, *30*, 337−343.

(30) Huang, B. G.; Shi, R. F.; Zhao, X. B.; ZHOU, G. Geological conditions of Paleozoic shale gas formation and its exploration potential in the South AnhuiLower Yangtze area. *J. China Coal Soc.* **2013**, *38*, 877−882.

(31) Miao, B. Study on reservoir-forming conditions and selection evaluation of shale gas in Dawuba Formation of Carboniferous in Qiannan, Guizhou. *Pet. Geol. Eng.* **2018**, *32*, 5−8.

(32) An, Y.; Fu, H.; Chen, H.; He, Y.; Fan, L.; Pan, Y. Physical property characteristics and controlling factors of shale gas reservoir in Lower Carboniferous Dawuba Formation in southern Guizhou: A case study of Changye 1 well reservoir. *Guizhou Geol.* **2015**, *32*, 181−189.

(33) He, J.; Wei, L.; Qian, Y.; Zhen, Q.; He, Y.; Guo, T.; Wang, Z.; Yang, P. Geological characteristics of shale gas in Jiusi Formation of Lower Carboniferous in Guizhou and optimal selection of favorable areas. *Chin. J. Geol.* **2017**, *1*, 203−217.

(34) Song, Y.; Hou, Y.; Liu, Y.; He, S.; Fan, Z.; Liang, Y. Study on thermal evolution and hydrocarbon generation history of dark shale of Lower Carboniferous Baizuo Formation in Qiannan Depression. *Pet. Geol. Exp.* **2018**, *40*, 226−232.

(35) Ross, D.; Bustin, R. M. Investigating the use of sedimentary geochemical proxies for paleoenvironment interpretation of thermally mature organic-rich strata: Examples from the Devonian−Mississippian shales, Western Canadian Sedimentary Basin. *Chem. Geol.* **2009**, *260*, 1−19.

(36) Curtis, J. B. Fractured shale-gas systems. *AAPG Bull.* **2002**, *86*, 1921−1938.

(37) Li, P.; Zhang, J.; Rezaee, R.; Dang, W.; Tang, X.; Nie, H.; Chen, S. Effect of adsorbed moisture on the pore size distribution of marine-continental transitional shales: Insights from lithofacies differences and clay swelling. *Appl. Clay Sci.* **2021**, *201*, No. 105926.

(38) Su, H.; Yang, R.; Cheng, W.; Zhang, Z. Shale Gas Accumulation Characteristics and Advantageous Area Analysis of Lower Carboniferous Dawuba Formation in Southwestern Guizhou. *J. Guizhou Univ.* **2017**, *34*, 41−46.

(39) Cao, J.; Yang, R.; Yin, W.; Hu, G.; Bian, L.; Fu, X. Mechanism of Organic Matter Accumulation in Residual Bay Environments: The Early Cretaceous Qiangtang Basin, Tibet. *Energy Fuels* **2018**, *32*, 1024.

(40) Liu, Y.; Liu, H. C.; Li, X. H. Simultaneous precise determination of 40 trace elements in rock samples using ICP-MS. *Geochemica* **1996**, *25*, 552−558.

(41) McLennan, S. M. Relationships between the trace element composition of sedimentary rocks and upper continental crust. *Geochem., Geophys., Geosyst.* **2001**, *2*, n/a.

(42) Amp, H. W. N.; Young, G. M. Early Proterozoic climates and plate motions inferred from major element chemistry of lutites. *Nature* **1982**, *299*, 715−717.

(43) Xu, X. T.; Shao, L. Y. Limiting factors in utilization of chemical index of alteration of mudstones to quantify the degree of weathering in provenance. *J. Palaeogeogr.* **2018**, *20*, 151−522.

(44) Bock, B.; Mclennan, S. M.; Hanson, G. N. Geochemistry and provenance of the Middle Ordovician Austin Glen Member (Normanskill Formation) and the Taconian Orogeny in New England. *Sedimentology* **1998**, *45*, 635−655.

(45) Yan, D.; Chen, D.; Wang, Q.; Wang, J. *Large-Scale Climatic Fluctuations in the Latest Ordovician on the Yangtze Block, South China*; Institute of Geology and Geophysics, Chinese Academy of Sciences, 2011; pp 599−602.

(46) McLennan, S. M.; Hemming, S.; McDaniel, D. K.; Hanson, G. N.; Johnsson, M. J.; Basu, A. Geochemical approaches to sedimentation, provenance, and tectonics. In *Processes Controlling the Composition of Clastic Sediments*; Geological Society of America, 1993; Vol. *284*.

(47) Dymond, J.; Erwin, S.; Mitch, L. Barium in Deep-Sea Sediment: A Geochemical Proxy for Paleoproductivity. *Paleoceanography* **1992**, *7*, 163−181.

(48) Bond, D. P. G.; Wignall, P. B. Pyrite framboid study of marine Permian−Triassic boundary sections: A complex anoxic event and its relationship to contemporaneous mass extinction. *Geol. Soc. Am. Bull.* **2010**, *122*, 1265−1279.

(49) Li, Y.; Yang, J.; Pan, Z.; Tong, W. Nanoscale pore structure and mechanical property analysis of coal: An insight combining AFM and SEM images. *Fuel* **2020**, *260*, 116352.

(50) Li, Y.; Wang, Z.; Pan, Z.; Niu, X.; Yu, Y.; Meng, S. Pore structure and its fractal dimensions of transitional shale: A cross-section from east margin of the Ordos Basin, China. *Fuel* **2019**, *241*, 417−431.

(51) Tian, S.; Yang, R. Lithofacies palaeogeography evolution and shale gas accumulation characteristics of the Early Carboniferous in Guizhou. *Journal of Chengdu University of Technology (Natural Science Edition)* **2016**, *43*, 291−299.

(52) ZHAN, S. Q.; DING, M. H.; LI, A. Y.; WANG, H.; et al. The application of wide field electromagnetic sounding method to exploration in carbonatite mountain areas of Guizhou Province. *Geophys. Geochem. Explor.* **2020**, *44*, 88−92.

(53) Zhi, L. I.; Ran, B.; Wang, M. H.; Guo, W.; Fa-Hao, L. I.; Wang, Y. Q.; University N. Jiangsu Survey G. G. Guiyang. Sedimentary Facies Analysis of Carboniferous Dawuba Group in Ziyun District of Guizhou Province. *Journal of Hebei GEO University* **2017**, *40*, 1−9.

(54) Ya-Yun, A. N.; Hong-Bin, F. U.; Chen, H. G.; Yong-Zhong, H. E.; Shu-Pan, L. U.; Pan, Y. J. Reservoir Property and Control Factors of Shale Gas of Dawuba Formation, Lower Carboniferous in South Guizhou—with Changye No.1 reservoir as an Example. *Guizhou Geol.* **2015**, *32*, 181−189.

(55) Tian, S. F.; Yang, R. D. Lithofacies and paleogeography evolution and characteristics of shale gas accumulation in Lower Carboniferous,Guizhou,China. *Journal of Chengdu University of Technology(Science & Technology Edition)* **2016**, *43*, 291−299.

(56) Ross, D. J.; Bustin, R. M. Investigating the use of sedimentary geochemical proxies for paleoenvironment interpretation of thermally mature organic-rich strata: Examples from the Devonian−Mississippian shales, Western Canadian Sedimentary Basin. *Chem. Geol.* **2009**, *260*, 1−19.

(57) Hatch, J. R.; Leventhal, J. S. Relationship between inferred redox potential of the depositional environment and geochemistry of the Upper Pennsylvanian (Missourian) Stark Shale Member of the Dennis Limestone, Wabaunsee County, Kansas, U.S.A. *Chem. Geol.* **1992**, *99*, 65−82.

(58) Jones, B.; Manning, D. A. C. Comparison of Geochemical Indices Used for the Interpretation of Palaeoredox Conditions in Ancient Mudstones. In *Chemical Geology*; Elsevier, 1994; Vol. *111*, pp 111−129.

(59) Wignall, P. B.; Myers, K. J. Interpreting benthic oxygen levels in mudrocks: A new approach. *Geology* **1988**, *15*, 452−455.

(60) Yan, D.; Wang, H.; Fu, Q.; Chen, Z.; He, J.; Gao, Z. Geochemical characteristics in the Longmaxi Formation (Early Silurian) of South China: Implications for organic matter accumulation. *Mar. Pet. Geol.* **2015**, *65*, 290−301.

(61) Algeo, T. J.; Li, C. Redox classification and calibration of redox thresholds in sedimentary systems. *Geochim. Cosmochim. Acta* **2020**, *287*, 8−26.

(62) Algeo, T. J.; Liu, J. A re-assessment of elemental proxies for paleoredox analysis. *Chem. Geol.* **2020**, *540*, 119549.

(63) Tribovillard, N.; Algeo, T. J.; Lyons, T.; Riboulleau, A. Trace metals as paleoredox and paleoproductivity proxies: An update. *Chem. Geol.* **2006**, *232*, 12−32.

(64) Algeo, T. J.; Maynard, J. B. Trace-element behavior and redox facies in core shales of Upper Pennsylvanian Kansas-type cyclothems. *Chem. Geol.* **2004**, *206*, 289−318.

(65) Dahl, T. W.; Ruhl, M.; Hammarlund, E. U.; Canfield, D. E.; Rosing, M. T.; Bjerrum, C. J. Tracing euxinia by molybdenum concentrations in sediments using handheld X-ray fluorescence spectroscopy (HHXRF). *Chem. Geol.* **2013**, *360-361*, 241−251.

(66) Helz, G. R.; Miller, C. V.; Charnock, J. M.; Mosselmans, J. F. W.; Pattrick, R. A. D.; Garner, C. D.; Vaughan, D. J. Mechanism of

molybdenum removal from the sea and its concentration in black shales: EXAFS evidence. *Geochim. Cosmochim. Acta* **1996**, *60*, 3631−3642.

(67) Zheng, Y.; Anderson, R. F.; van Geen, A.; Fleisher, M. Q. Remobilization of authigenic uranium in marine sediments by bioturbation. *Geochim. Cosmochim. Acta* **2002**, *66*, 1759−1772.

(68) Algeo, T. J.; Tribovillard, N. Environmental analysis of paleoceanographic systems based on molybdenum−uranium covariation. *Chem. Geol.* **2009**, *268*, 211−225.

(69) Bruland, K. W. Trace Elements in Sea-water. *Chem. Oceanogr.* **1983**, *49*, 157−220.

(70) Niu, Y. F.; Jin-Lin, L. U.; Huang, Z. H. Discrimination of sedimentary environment by the characteristics of geochemical elements. *World Nonferrous Metals* **2018**, *01*, 287−289.

(71) Ding, J.; Zhang, J.; Tang, X.; Huo, Z.; Han, S.; Lang, Y.; Zheng, Y.; Li, X.; Liu, T. Elemental Geochemical Evidence for Depositional Conditions and Organic Matter Enrichment of Black Rock Series Strata in an Inter-Platform Basin: The Lower Carboniferous Datang Formation, Southern Guizhou, Southwest China. *Minerals* **2018**, *8*, 509.

(72) Schoepfer, S. D.; Shen, J.; Wei, H.; Tyson, R. V.; Ingall, E.; Algeo, T. J. Total organic carbon, organic phosphorus, and biogenic barium fluxes as proxies for paleomarine productivity. *Earth-Sci. Rev.* **2015**, *149*, 23−52.

(73) Boyle, E. A.; Sclater, F. R.; Edmond, J. M. The distribution of dissolved copper in the Pacific. *Earth Planet. Sci. Lett.* **1977**, *37*, 38−54.

(74) Guillard, R. R. L.; Anderson, M. A.; Morel, F. M. M. Growth limitation of a coastal diatom by low zinc ion activity. *Nature* **1978**, *276*, 70−71.

(75) Dehairs, F.; Stroobants, N.; Goeyens, L. Suspended barite as a tracer of biological activity in the Southern Ocean. *Mar. Chem.* **1991**, *35*, 399−410.

(76) Goeyens, L. *The Biochemistry of Barium in the Southern Ocean*; 1989.

(77) Yang, T.; Cao, Y.; Wang, Y.; Zhang, S. Types, sedimentary characteristics and genetic mechanism of deep-water gravity flow: A case study of the middle member of the third member of Shahejie Formation in Jiyang depression. *Acta Pet. Sin.* **2015**, *36*, 1048−1059.

(78) Fu, Y.; Zhongcheng, L.; Pu, W.; Yijuan, Q.; Zhenjun, W.; Ji, Y.; Huang, L.; Luo, J.; Zhidong, B. Sedimentary characteristics and controlling factors of slump gravity flow in delta front: A case study of Qing1 Member in Da 'an area, Songliao Basin. *Lithologic Reservoirs* **2021**, *33*, 198−208.

(79) Embry, A. F. Transgressive−regressive (T−R) sequence analysis of the Jurassic succession of the Sverdrup Basin, Canadian Arctic Archipelago. *Can. J. Earth Sci.* **1993**, *30*, 301−320.

(80) Potter, P. E.; Shimp, N. F.; Witters, J. Trace Elements in Marine and Fresh-Water Argillaceous Sediments. *Soil Sci.* **1965**, *99*, 286.

(81) Tribovillard, N.; Algeo, T. J.; Baudin, F.; Riboulleau, A. Analysis of marine environmental conditions based onmolybdenum−uranium covariation—Applications to Mesozoic paleoceanography. *Chem. Geol.* **2012**, *324-325*, 46−58.

(82) Zabel, M.; Schneider, R. R.; Wagner, T.; Adegbie, A. T.; de Vries, U.; Kolonic, S. Late Quaternary Climate Changes in Central Africa as Inferred from Terrigenous Input to the Niger Fan. *Quater. Res.* **2001**, *56*, 207−217.

(83) Goodarzi, F.; Nina, N. G.; Malachowska, A. Elemental composition, environment of deposition of the Lower Carboniferous Emma Fiord Formation oil shale in Arctic Canada. *Int. J. Coal Geol.* **2021**, *244*, No. 103715.

(84) Goodarzi, F. Comparison of the geochemistry of lacustrine oil shales of Mississippian age from Nova Scotia and New Brunswick, Canada. *Int. J. Coal Geol.* **2020**, *220*, No. 103398.

(85) Goodarzi, F.; Gentzis, T.; Sanei, H.; Pedersen, P. K. Elemental composition and organic petrology of a Lower Carboniferous-age freshwater oil shale in Nova Scotia, Canada. *ACS Omega* **2019**, *4*, 20773−20786.

(86) Kasanzu, C.; Maboko, M.; Manya, S. Geochemistry of fine-grained clastic sedimentary rocks of the Neoproterozoic Ikorongo Group, NE Tanzania: Implications for provenance and source rock weathering. *Precambrian Res.* **2008**, *164*, 201−213.

(87) Passey, Q. R.; Bohacs, K. M.; Esch, W. L.; Klimentidis, R.; Sinha, S. *From Oil-Prone Source Rock to Gas-Producing Shale Reservoir − Geologic and Petrophysical Characterization of Unconventional Shale-Gas Reservoirs*, International Oil and Gas Conference and Exhibition in China, 2010.